The Solomon Sea: its circulation, chemistry, geochemistry and biology explored during two oceanographic cruises

Alexandre Ganachaud, Sophie Cravatte, Janet Sprintall, Cyril Germineaud, Marion Alberty, Catherine Jeandel, Gérard Eldin, Nicolas Metzl, Sophie Bonnet, Mar Benavides, et al.

ELEMENTA
Science of the Anthropocene

Ganachaud, A, et al 2017 The Solomon Sea: its circulation, chemistry, geochemistry and biology explored during two oceanographic cruises
Elem Sci Anth, 5: 33, DOI: https://doi.org/10.1525/elementa.221

RESEARCH ARTICLE

The Solomon Sea: its circulation, chemistry, geochemistry and biology explored during two oceanographic cruises

Alexandre Ganachaud[*], Sophie Cravatte[*,†], Janet Sprintall[‡], Cyril Germineaud[*], Marion Alberty[‡], Catherine Jeandel[*], Gerard Eldin[*], Nicolas Metzl[‖], Sophie Bonnet[§], Mar Benavides[§], Lars-Eric Heimburger[§], Jérôme Lefèvre[†], Susanna Michael[¶], Joseph Resing[¶], Fabien Quéroué[**], Géraldine Sarthou[**], Martine Rodier[††], Hugo Berthelot[‡‡], François Baurand[§§], Jacques Grelet[§§], Takuya Hasegawa[‖‖], William Kessler[¶¶], Moyep Kilepak[***], François Lacan[*], Emilien Privat[*], Uwe Send[‡], Pieter Van Beek[*], Marc Souhaut[*] and Jeroen E. Sonke[†††]

The semi-enclosed Solomon Sea in the southwestern tropical Pacific is on the pathway of a major oceanic circuit connecting the subtropics to the equator via energetic western boundary currents. Waters transiting through this area replenish the Pacific Warm Pool and ultimately feed the equatorial current system, in particular the equatorial undercurrent. In addition to dynamical transformations, water masses undergo nutrient and micronutrient enrichment when coming in contact with the coasts, impacting the productivity of the downstream equatorial region. Broadscale observing systems are not well suited for describing the fine-scale currents and water masses properties in the Solomon Sea, leaving it relatively unexplored. Two multidisciplinary oceanographic cruises were conducted in the Solomon Sea region, the first in July–August 2012 and the second in March 2014, by investigators from France and the United States. The experimental approach combined physical, chemical, geochemical and biogeochemical analyses, providing access to a wide range of space and time scales of the circulation. This collection of data allows describing the fine-scale structure of the currents and the water properties, transformations and mixing from the surface to the sill depth in the Solomon Sea and in the straits connecting it to the equator. Ocean-margin exchanges were documented through a comprehensive sampling of trace elements and isotopes as efficient tracers of natural fertilization processes. As air chemistry is largely impacted by the regional volcanic plumes, rainwater pH was also sampled. Dinitrogen fixation rates were measured and found to be among the highest in the global ocean, highlighting this region as a hot spot of nitrogen fixation. This study provides an overview of the climatic context during both cruises and the physical circulation and water masses properties. It provides a comprehensive description of all measurements made onboard, and presents preliminary results, aiming to serve as a reference for further physical, geochemical and biogeochemical studies.

Keywords: Solomon Sea; Low latitude western boundary currents; Biogeochemistry

* LEGOS, Université de Toulouse, CNES, CNRS, IRD, (Toulouse), FR
† IRD, LEGOS, UMR5566, IRD, CNRS, UPS, CNES, Nouméa, NC
‡ Scripps Institution of Oceanography, La Jolla, CA, US
§ Mediterranean Institute of Oceanography (MIO), Aix Marseille Université, CNRS/INSU, Université de Toulon, IRD, UM 110, Noumea, NC
‖ Sorbonne Universités (UPMC, Univ Paris 06) CNRS-IRD-MNHN, LOCEAN/IPSL, Paris, FR
¶ Joint Institute for the Study of the Atmosphere and Ocean (JISAO) and Pacific Marine Environmental Laboratory (PMEL), Seattle, WA, US
** Laboratoire des Sciences de l'Environnement Marin, UMR CNRS-IRD-UBO-IFREMER 6539/LEMAR/IUEM, Technopole Brest Iroise, Place Nicolas Copernic, Plouzané, FR
†† Ecosystèmes Insulaires Océaniens, UMR IRD-Université de la Polynésie Française-Institut Malarmé-Ifremer, Centre IRD de Tahiti, PF
‡‡ Mediterranean Institute of Oceanography (MIO), Aix Marseille Université, CNRS/INSU, Université de Toulon, IRD, UM 110, Marseille, FR
§§ US-IMAGO, IRD, Centre IFREMER, Plouzané, FR
‖‖ Japan Agency for Marine-Earth Science and Technology, Yokosuka, JP
¶¶ Pacific Marine Environmental Laboratory, National Oceanic and Atmospheric Administration, Seattle, WA, US
*** University of Papua New Guinea, Port Moresby, PG
††† GET, UMR5563, University of Toulouse, IRD, CNRS, UPS, CNES, Toulouse, FR

Corresponding author: Alexandre Ganachaud (Alexandre.Ganachaud@legos.obs-mip.fr)

Introduction

The Solomon Sea is a semi-enclosed sea located at the western boundary of the equatorial Southwest Pacific Ocean, between Papua New Guinea and the Solomon Islands (**Figure 1**). Suspecting the importance of the Solomon Sea circulation to the general Pacific circulation, Lindstrom et al. (1987) made two surveys in 1985 and 1986 that revealed large and vigorous transports toward the equator. This region appeared as an essential pathway for waters originating from mid-to high latitudes and joining the western equatorial Pacific and the equatorial current system. Water properties indicated that the Solomon Sea was in particular the major source of the Equatorial Undercurrent (Tsuchiya et al., 1989), and thereby of the downstream surface waters of the cold tongue in the eastern equatorial Pacific. Since then, the area had essentially only been surveyed by underway shipboard current profilers during research vessel transits or geophysical cruises (Cravatte et al., 2011).

Recently, the CLIVAR Southwest Pacific Ocean Circulation and Climate Experiment (SPICE) pinpointed the region as a key passageway for the low-latitude western boundary currents, providing important components for the oceanic and climatic variability of the equatorial Pacific at interannual and decadal time scales (Ganachaud et al., 2014). Water mass mixing, and geochemical and biogeochemical enrichments in the Solomon Sea may indeed impact the downstream surface waters and the productivity of the equatorial cold tongue.

The oceanic conditions in the Solomon Sea are distinctive in several ways. First, strong currents interacting with numerous islands and straits impact water properties (Melet et al., 2011). Then, water masses coming in contact with the coasts undergo not only dynamical transformations but also enrichments of macro-and micro-nutrients and trace elements through land/sea exchange, or *boundary exchanges* (BE) (Grenier et al., 2011), including river discharge, shelf inputs and submarine groundwater discharges. Trace elements and their isotopes that are injected from BE provide information on transformation and fate of particles and on water masses as well as mixing. Quantifying these BE is a priority of the international GEOTRACES program (e.g., Grenier et al., 2014).

In the context of the SPICE program, two major multidisciplinary cruises were organized inside the Solomon Sea: the Pandora cruise in July–August 2012, and the MoorSPICE cruise in March 2014. Pandora documented the physics, geochemistry, biology and chemistry of the area (**Figure 2**) for full cruise track from New Caledonia. MoorSPICE partly repeated the hydrographic measurements, then explored the Bismarck Sea to the North (**Figure 2**). The main objectives of these two cruises were to document the circulation, mixing, water mass transformations and pathways; to document the chemistry, geochemistry, and the enrichment of waters in the area. In addition, it has been recently shown that the Solomon Sea is a place of large, but essentially undocumented nitrogen fixation (Bonnet et al., 2009): these cruises were an opportunity to better document N_2 fixation. They also allowed the first evaluation of both anthropogenic carbon and ocean acidification in the region.

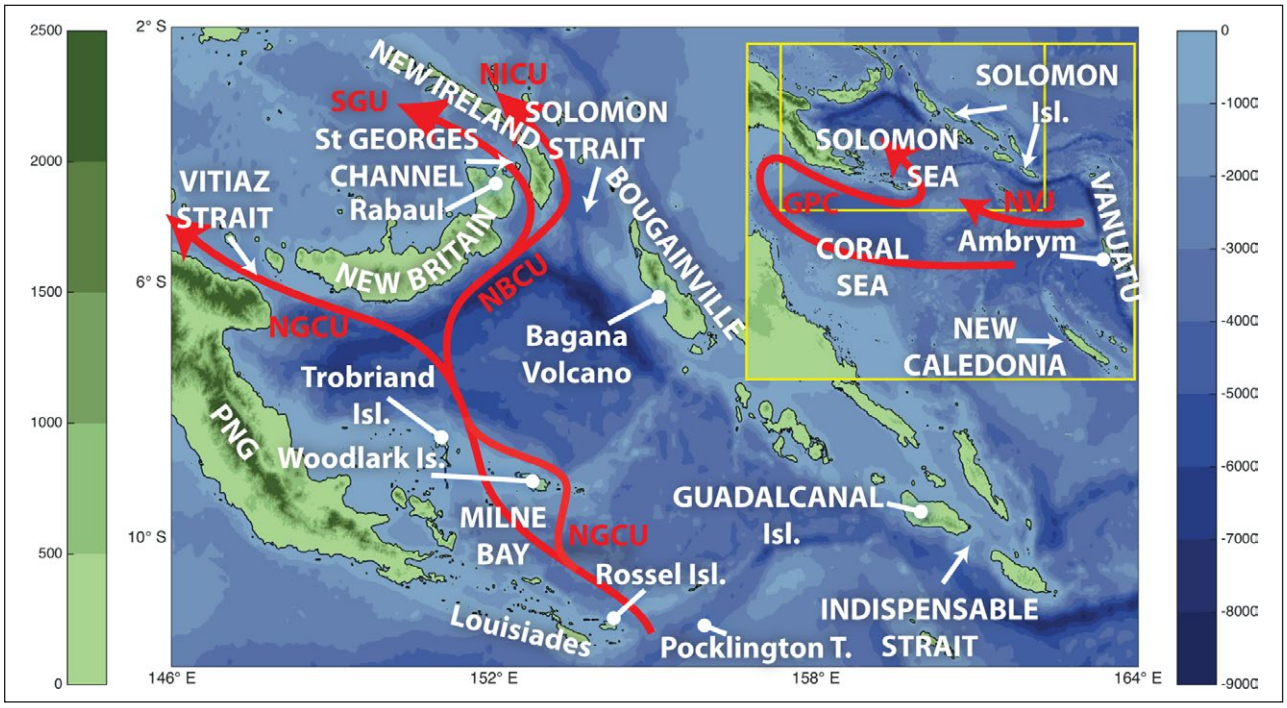

Figure 1: Solomon Sea topography, bathymetry, main points of interest (white text) and oceanic currents (red text). (Inset): Southwest Pacific topography. Currents are as follows: New Guinea Coastal Undercurrent (NGCU); New Britain Coastal Undercurrent (NBCU); St. Georges Channel Undercurrent (SGU); New Ireland Coastal Undercurrent (NICU); Gulf of Papua Current (GPC); North Vanuatu Jet (NVJ). PNG stands for Papua New Guinea. Isl. indicates "island"; Pocklington T. indicates Pocklington Through. DOI: https://doi.org/10.1525/elementa.221.f1

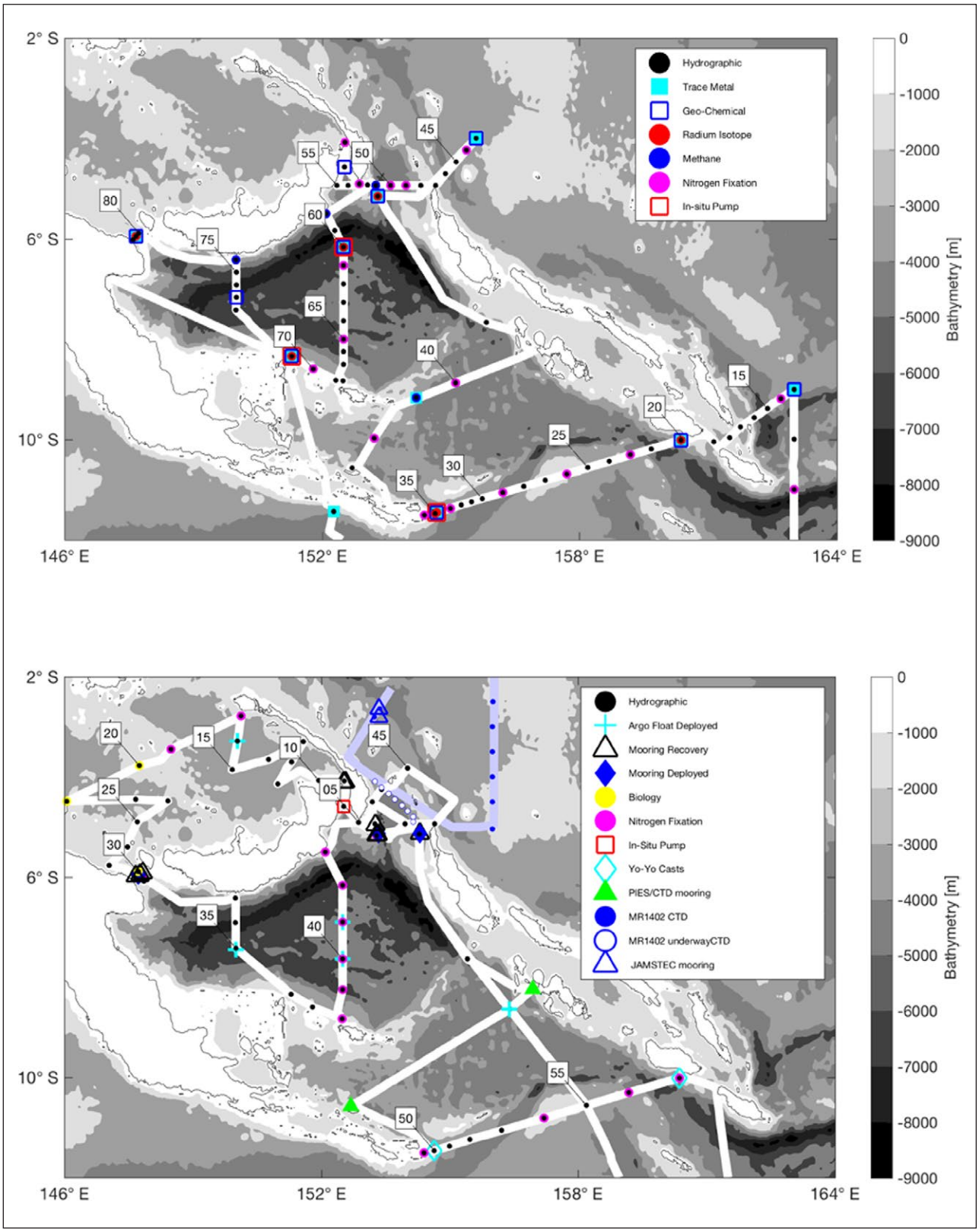

Figure 2: Cruise tracks and sampling strategies for the two oceanographic cruises in the Solomon Sea. The Pandora cruise **(a)** took place during July–August 2012 aboard the R/V *l'Atalante*, French Oceanographic Fleet; MoorSPICE and MR14-02 cruises **(b)** took place during February–March 2014 aboard, respectively the R/V *Thompson*, USA and the R/V *Mirai*, Japan. Both Pandora and MoorSPICE cruises departed and arrived in New Caledonia while MR14–02 departed and arrived in Japan. Each station/cast had specific protocols and characteristics, as indicated in the legend box. For clarity, mooring positions are reported only on panel (b). Station numbers are indicated every 5th station. DOI: https://doi.org/10.1525/elementa.221.f2

The objectives of this paper are to present the general context of these cruises and to provide an initial overview for subsequent more detailed analyses by physical oceanographers, geochemists and biologists. The scientific rationale for these cruises and the measurements made are presented. The climatic context is provided, and key results inferred from observations made during these cruises are also summarized.

Background

Circulation and water characteristics

Recent targeted efforts in the context of the SPICE program have helped to understand aspects of the mean oceanic circulation within the Solomon Sea from a diverse source of observations (vessel-mounted current profiler compilations, gliders, drifters and hydrological data) and modeling studies (Ganachaud et al., 2014). All previous works agree on the following mean circulation pattern: the bulk of thermocline transport into the Solomon Sea enters through the southern opening of the Solomon Sea where the Gulf of Papua Current joins the North Vanuatu Jet (NVJ) in forming the low latitude western boundary current called the New Guinea Coastal Undercurrent (NGCU) (**Figure 1**); (e.g., Melet et al., 2010; Gasparin et al., 2012; Kessler and Cravatte, 2013). The NGCU travels equatorward, splitting around Woodlark Island, then rejoins before it bifurcates just south of New Britain. The westward branch exits the Solomon Sea through Vitiaz Strait while the eastward branch travels along the coast of New Britain as the New Britain Coastal Undercurrent (NBCU) (Cravatte et al., 2011). The majority of the NBCU exits through Solomon Strait and the remainder passes through St. Georges Channel. In the near surface, the mean circulation is slightly different, with water entering the Solomon Sea through Solomon Strait and exiting southward through the southern entrance (Melet et al., 2010; Hristova and Kessler, 2012). Surface velocities can also be weaker than subsurface, with strong seasonal variations (Cravatte et al., 2011). At deeper levels, the circulation in the Solomon Sea and straits is quasi unknown.

Mean total transport through the Solomon Sea is estimated to be ~30 Sv above 1300 m (Gasparin et al., 2012). The strength of the currents varies on a seasonal timescale with the strongest equatorward flows from June to September during the southeasterly monsoon (Cravatte et al., 2011; Hristova and Kessler, 2012). Currents also vary on El Niño Southern Oscillation (ENSO) timescale in the upper 250 m, with transports increasing during El Niño events and decreasing – or even reversing – during La Nina events (Davis et al., 2012; Melet et al., 2013). Additionally, surface and subsurface mesoscale eddies and submesoscale features dominate instantaneous current fields (Djath et al., 2014; Gourdeau et al., 2014; Hristova et al., 2014).

Water masses, currents, their variation and the partition of their transports between the different straits have therefore been inferred from numerical simulations and scattered measurements mainly confined to the upper 300 m. However, we have not as yet had simultaneous measurements of physics and geochemistry, and our understanding of the internal and deep Solomon Sea has been extremely limited by the lack of measurements.

N_2 fixation and primary production

The Solomon Sea is an interesting site for its specific biology and chemistry, in particular, atmospheric dinitrogen (N_2) fixation. N_2 fixation is the process by which N_2 is reduced to ammonia by specialized microbes termed diazotrophs. This process is the major external source of nitrogen for the ocean, even more important than riverine and atmospheric inputs (Gruber, 2004). N_2 fixation thus provides nitrogenous nutrients for phytoplankton communities and contributes to carbon dioxide (CO_2) uptake and climate regulation (Karl et al., 2002). The South Pacific Ocean has been ranked as the second major basin contributing to global N_2 fixation after the Indian Ocean (Luo et al., 2012), although studies performed in the South Pacific are much less numerous than those performed, for example, in the Indian (Luo et al., 2012), in the North Atlantic (Benavides and Voss, 2015) and the North Pacific Oceans (Karl et al., 1997; Dore et al., 2002).

The tropical Pacific is characterized by a strong zonal gradient in nutrient distribution, with the eastern basin affected by the cold equatorial tongue where nutrient availability is higher but trace metals limit primary production (Aufdenkampe et al., 2002; Le Bouteiller, 2003), and the western basin dominated by a warm pool where metals are available through land runoff, hydrothermalism, and volcanic activity (Labatut et al., 2014). In the western Pacific, the permanent water column stratification inhibits nutrient upwelling (Pena et al., 1994) and N_2 fixation appears as the main source of nitrogenous nutrients for primary production (Yoshikawa et al., 2005; Bonnet et al., 2009). This zonal pattern is also reflected in N_2 fixation activity and in the diversity of diazotrophs, with low N_2 fixation rates in the eastern side of the South Pacific (Raimbault and Garcia, 2008) dominated by heterotrophic diazotrophs (Bonnet et al., 2008; Halm et al., 2012), and potentially high rates provided by autotrophic diazotrophs on the western side (Bonnet et al., 2009; Moisander et al., 2010). However, very few studies have quantified N_2 fixation in the Southwest Pacific, in particular in the Solomon Sea, which presents ideal temperature conditions for diazotrophs to bloom extensively (Bonnet et al., 2017).

Trace elements and sulfur

Numerous processes that could affect water properties are occurring at the land-ocean interface and within the water column. These include advective, diffusive and turbulent transports; biological uptake; remineralization; river runoff; dissolution of lithogenic minerals and precipitation of authigenic ones (i.e., precipitated locally within the water column); adsorption on particles followed by scavenging or desorption from particles followed by the release of the chemical species. Understanding the sources of these trace elements is fundamental for their integration in any model coupling circulation

and biogeochemistry. Chemical elements and isotopes identified that help to constrain the nature and rate of these processes are considered as "oceanic" tracers and part of the GEOTRACES core parameters (GEOTRACES science plan, online at http://www.geotraces.org). The Coral and Solomon Seas are of particular interest to provide indications of these processes because of their energetic dynamics, where boundary exchange is suspected to be of importance (Lacan and Jeandel, 2005; Grenier et al., 2013; Jeandel and Oelkers, 2015).

The surface deposition from volcanic plumes is also a potential source of various species. Papua New Guinea (PNG), the Solomon Islands and Vanuatu form the Melanesian volcanic arc with large emitters of volcanic species and sulfate precursors (Bani et al., 2012; McCormick et al., 2012). Air chemistry of the marine boundary layer and free troposphere of the Solomon Sea is largely impacted by volcanic plumes from PNG volcanoes (i.e., Rabaul and Bagana, located in New Britain and Bougainville Islands, respectively; **Figure 1**) but also from remote volcanic plumes. The Vanuatu Ambrym volcano is ranked as one of the top emitters, producing between 8% and 17% of global volcanic fluxes of SO_2, HCl, HF, HBr, Hg and ^{210}Po (Allard et al., 2015).

Data sets on cloud chemistry and pH in wet deposition are very limited in the region. Nagamoto et al. (1990) provided the first survey of cloud chemistry across the Western Pacific and recorded rainwater pH values in the range of 5 to 6 in the equatorial and remote island region north of Solomon Islands. They suggested a role of the biogenic source (dimethyl sulfide) in rain composition. But over Vanuatu, Vetch and Haefeli (1997) measured a pH of 2 in rainwater 4 km away from Ambrym's crater (**Figure 1**). Lefevre et al. (2015) showed that Ambrym is the main source of sulfur species in the Coral and Solomon Seas, with a similar contribution to the regional sulfur budget as dimethyl sulfide (DMS) emitted from marine organisms.

The methylmercury (MeHg) cycle is also unclear; in particular, we do not know whether MeHg is produced primarily in marine sediments and subsequently advected into the open ocean or whether it is produced in situ in the oceanic water column, during the remineralization of sinking organic matter (Fitzgerald et al., 2007; Mason et al., 2012).

Carbon cycle

The global ocean absorbs about 30% of the annually-emitted anthropogenic carbon slowing the rapid accumulation of CO_2 in the atmosphere that has recently reached 400 ppm (global CO_2 mean in March 2015, Le Quéré et al., 2015). But the ocean carbon uptake leads to a decrease in pH, the so-called "other" CO_2 problem of ocean acidification, which will have a harmful impact on marine organisms and ecosystems. Since pre-industrial times, the mean pH in the surface ocean has dropped by about 0.1 units. In order to follow both the anthropogenic CO_2 penetration in the ocean and changes in acidification, observations are needed to be conducted regularly in open oceans, marginal seas and coastal Zones. Very few observations of the inorganic carbon system have been conducted previously in the Coral and Solomon Seas (Suzuki et al., 2013; Lauvset et al., 2016; Olsen et al., 2016). It is thus interesting to explore the CO_2 system in this area (also referred as southeastern part of the Coral Triangle), including the anthropogenic CO_2 penetration and associated ocean acidification and compare our new observations with previous analysis conducted in open ocean tropical and subtropical zones (e.g., Alvarez et al., 2009). Interestingly, this region, part of the so-called North Australia region in the project called MARCATS (MARgins and CATchments Segmentation), presents large uncertainty in estimates of air-sea CO_2 fluxes whether depending on data-based method (CO_2 source) or ocean biogeochemical models (CO_2 sink) (Bourgeois et al., 2016). A recent study using data-based reconstruction (Lenton et al., 2016) also suggests low pH in this region (8.03 – 8.05) but authors also concluded that at present the Coral Sea is not experiencing marginal conditions with respect to ocean acidification (values of the aragonite saturation state <3.5).

Data and methods

Most data analyzed in this paper originate from the two research cruises: Pandora carried out aboard the French research vessel *l'Atalante* (also recorded as GEOTRACES cruise GP12), and the MoorSPICE cruise aboard US research vessel *Thomas G.* Thompson. As part of the Tropical Ocean Climate Study (TOCS) project, a cruise took place aboard the R/V *Mirai* (MR14–02) in February 2014, around the New Ireland (**Figure 2b**). This cruise was conducted by the Japan Agency for Marine-Earth Science and Technology (JAMSTEC) in order to explore the oceanic leakage between the Solomon Sea and the western equatorial Pacific through the NICU pathways (**Figure 2b**). Data acquired during this cruise are not discussed here.

Pandora Cruise, July-August 2012

The R/V *l'Atalante* departed Nouméa, New Caledonia, on 28 June 2012, and returned to port on 6 August (**Figure 2a**; see Figure S1a for a larger-scale map). Scientific equipment included two SBE-911 + CTD/Rosette systems. The primary *standard* rosette was used at all stations outfitted with duplicated temperature-conductivity-oxygen SBE sensors, a Chelsea Aqua3 fluorometer, a Wetlab C-star transmissometer and a pair of RDI built Lowered-Acoustic Doppler Current Profilers (L-ADCP) attached to the CTD frame (150 kHz and 300 kHz, down- and up-looking, respectively) to measure currents along the rosette profile. The rosette was fitted with 22 × 12L Niskin bottles to obtain water samples for the standard parameters (see below).

The secondary *clean* rosette was designed for obtaining uncontaminated samples for trace metals, with a titanium CTD body and epoxy coated frame, and included one set of SBE temperature-conductivity-oxygen sensors, a Wetlab Westar fluorometer and 12L Go-Flo bottles. A set of 7 Maclane or Challenger in situ pumps for sampling of particulate matter was deployed at 5 stations on a

hydrography wire. Underway continuous recordings are summarized in Table S1 as well as specific discrete sampling.

The Pandora cruise track included a meridional section along 163°E, from 18°S to 9°S, to sample incoming waters from the SEC (**Figure 2a**) followed by a section across the southern entrance of the Solomon Sea that closely followed a 2007 cruise track (Gasparin et al., 2012). Three more sections across the Solomon Sea were conducted to follow the paths and transformations of water masses (**Figure 2a**). Other sections included one on the eastern side of the Solomon Islands and two across Solomon and Vitiaz Straits. Details of the parameters sampled during stations are given in Table S2. Along the cruise track, eleven long duration stations with repeated casts (3–39 h, Table S2, last row) allowed the necessary large-volume water samplings required for geochemical analyses. Moreover, the repeated CTD casts during these stations provided additional information on the high frequency variability of properties and currents. Overall, measurements were made at 83 stations, for a total of 170 casts, including 30 clean sample casts, and 6 on situ pump deployments (**Figure 2a**).

A total of 9 moorings were deployed over the northern exit channels of Vitiaz and Solomon strait, and in St. Georges Channel from 2012 to March 2014 (MoorSPICE cruise), with two CTD moorings on either side of the southern mouth of the Solomon Sea since 2012. These latter two moorings were combined with bottom pressure inverted echosounders to capture the geostrophic transport between these two endpoint moorings. They will remain deployed (with some intermediate servicing) until summer 2017, and are part of a boundary current transport monitoring system measuring the inflow into the Solomon Sea using gliders (Davis et al., 2012).

MoorSPICE Cruise, February—March 2014

The MoorSPICE cruise aboard the R/V Thomas G. *Thompson* was carried out from 28 February 2014 to 31 March 2014. Scientific equipment included a dual set of temperature-conductivity-oxygen SBE-911+ CTD, a Wetlab ECO fluorometer, a Wetlab C-star transmissometer and a pair of RDI L-ADCPs attached to the CTD frame (300 kHz down- and up-looking). The rosette was fitted with 24 12–L Niskin bottles.

The ship directly sailed from Nouméa to the Solomon Strait and St. Georges Channel to recover the moorings previously deployed during the Pandora cruise; and a number of CTD stations were reoccupied. A saw-tooth pattern across the Bismarck Sea was then performed, in an area with poor in situ data coverage. The cruise continued through Vitiaz Strait, where mooring work was done. Then the track closely followed that of Pandora across the northern section of the Solomon Sea (in a reversed pattern). At the entrance to the Solomon Sea, most of the Pandora stations were reoccupied. Upon reaching Guadalcanal the ship sailed back to Nouméa. Overall, 57 stations were surveyed, some of them repeated, for a total of 78 casts (**Figure 2b**). Details of underway and on-station sampled parameters are given in Tables S1 to S3 (Section *Supplemental Material*). There were 6 Argo deployments, 9 moorings that were deployed during Pandora were recovered, and 4 additional moorings were re-deployed.

Physical parameters

For both cruises, data processing followed the GO-SHIP guidelines (online at http://www.go-ship.org/HydroMan.html). Temperature and conductivity sensors were calibrated by the manufacturer soon after the cruises. Calibration parameters were applied after checking agreement with salinity bottle samples. Every CTD cast was checked for spikes that might be due to particulate matter in the sensor circuits or electrical problems, and flagged accordingly. Dissolved oxygen sensor data were adjusted by comparison with a Winkler titration determination of water samples (Langdon, 2010; Uchida et al., 2010; Saout-Grit et al., 2015).

Shipboard ADCP velocity data were processed and calibrated using the CODAS software (online at http://currents.soest.hawaii.edu). LADCP velocity data was processed using the GEOMAR/LDEO software v10.8 (Visbeck, 2002). Continuous surface temperature and salinity as well as basic meteorological data were recorded by both ships using the underway thermosalinograph and meteorological systems, respectively.

Moorings

During the July 2012 cruise, nine moorings were deployed in Vitiaz and Solomon straits, and St. Georges Channel (**Figure 2b**). Moorings in the straits were recovered and four of them were re-deployed in Vitiaz Strait and Solomon Strait during the March 2014 cruise, and recovered in August 2015. They provided continuous measurements of near full-depth temperature, salinity and velocity. Two subsurface ADCP moorings were also deployed off the eastern coast of New Ireland Island in August 2012 during TOCS MR12–03 cruise; they were recovered in February 2014 during TOCS MR14–02 cruise. They provided continuous current velocity data from near surface to subsurface. Two moorings were also deployed on either side of the southern entrance of the Solomon Sea in 2012 (**Figure 2b**). These moorings were part of a boundary current heat transport monitoring system also using gliders and pressure inverted echosounders (Davis et al., 2012). These data will be presented in future papers.

Nutrients

Dissolved nutrients (N, P, Si) were sampled and analyzed at high precision following the GO-SHIP guidelines (Hydes et al., 2010) but based on pasteurization (Aminot and Kerouel, 1995; Daniel et al., 2012). Pasteurized samples were analyzed on a SEAL-AA3 automated Segmented Flow Analysis, following (Aminot and Kerouel, 2007; Hydes et al., 2010).

Carbonates

Discrete samples for total dissolved inorganic carbon (DIC) and total alkalinity (TA) were collected at selected stations, poisoned with $HgCl_2$ after sampling and measured back at

LOCEAN laboratory in Paris-France using a potentiometric titration (e.g., Metzl et al., 2010). For calibration, we used certified reference material (CRM, Batch #119) provided by Prof A. Dickson (Scripps Institution of Oceanography, San Diego, USA). The accuracy of DIC and TA are estimated to be ±2.6 μmol kg^{-1} and ±2.1 μmol kg^{-1}, respectively. Using DIC/TA pairs, other inorganic carbon properties were calculated (Pierrot et al., 2011), including the fugacity of CO_2 (fCO_2), carbonate ions, calcium carbonate solubility (for aragonite and calcite), and pH. For all derived calculations we used recommended constants K1 and K2 from Mehrbach et al. (1973) refit by Dickson and Millero (1987; 1989), and pH is seawater scale.

Acid precipitation

The presence of volcanogenic acidic sulfur was monitored using 30 rainwater samples during Pandora. pH and temperature in rainwater were measured using a rain gauge fixed on the fore deck, which provided a simple and affordable measurement. A glass electrode was used to determine pH values in rain samples immediately after collection (WTW 3110 pH meter). The pH readings were standardized with commercial buffer solutions.

N_2 fixation, primary production

The abundance of different diazotroph phylotypes was assessed through quantitative polymerase chain reaction (qPCR) counts of the *nifH* gene (encoding for a subunit of the nitrogenase enzyme, responsible for the N_2 fixation activity) as previously described (Church et al., 2005; Moisander et al., 2008). For the purpose of this study, only the main phylotypes are reported (i.e., *Trichodesmium* and the sum of unicellular diazotrophic cyanobacteria, UCYN). N_2 fixation and primary production were measured at four depths: 5, 50, 100, 150 m during Pandora (Table S2); and 5, 15, 30, 70 m during MoorSPICE (Table S3) using $^{15}N/^{13}C$ dual isotopic labeling and in situ-simulated 24–h incubation as described in Bonnet et al. (2015); Berthelot et al. (2017).

Trace elements

During Pandora (also GEOTRACES GP12), a comprehensive group of trace element samples and some isotopes (TEIs) were for subsequent measurements. They are listed in the appendix together with their role as geochemical tracers. Al, Mn, Hg speciation and dissolved Fe were available for this study.

Dissolved iron (dFe) samples were collected using a trace metal clean rosette and Go-Flo bottles with a slight N_2 overpressure to force filtration through 0.2 μm filter cartridges (Sartrobran-300, Sartorius). They were acidified to pH 2.0 with ultrapurQR hydrochloric acid (HCl, Merck) and analyzed on board after at least 24 h by flow injection with chemiluminescence detection (Sarthou et al., 2007). Samples for total and dissolved aluminum (Al) and manganese (Mn) were collected into 100 mL LDPE bottles. Total samples were collected directly into the sample bottle, while dissolved samples were collected after their passage through 0.2 μm cellulose acetate Sartobran-300 capsule filters. Samples were acidified to pH < 7 with 12 N Optima HCl at least one week prior to analysis. Al and Mn were determined by flow injection analysis using fluorimetric (Resing and Measures, 1994), and spectrophotometric (Resing and Mottl, 1992) detection, respectively. The manganese chemistry was modified by adding 4 g of nitrilo tri-acetic acid per liter of reaction buffer.

Total Hg (tHg) and methylmercury (MeHg) were measured according to Heimburger et al. (2015). The 9 profiles sampled during the Pandora cruise consisted of 89 unfiltered acidified (HCl 0.4%, v/v) samples.

Climatic context during Pandora and MoorSPICE cruises

The Solomon Sea is a region subject to significant annual variability (influenced by the Australian monsoon), interannual variability (linked to El Niño Southern Oscillation cycles), and intraseasonal variability (linked essentially to Madden-Julian Oscillation events, cyclones and synoptic westerly wind events). The Pandora and MoorSPICE cruises sampled two contrasted seasons, associated with significant changes in winds and precipitation. Pandora took place during the dry strong-trade winds season (June—November), in July—August 2012, and MoorSPICE during the wet weak-trade winds season (December—May), in March 2014. At this time of year, the SPCZ is fully developed over the Solomon Sea and the winds weaken or even reverse direction to become northwesterly.

The Pandora cruise occurred following the 2011 La Niña event and coincided with a return to neutral state, also present during the MoorSPICE cruise (**Figure 3**). The MoorSPICE cruise followed a series of strong equatorial westerly wind bursts and corresponding downwelling eastward Kelvin waves, associated with the onset of the "aborted 2014 El Niño" (Menkes et al., 2014; McPhaden et al., 2015).

In general, El Niño periods in the Coral Sea—Solomon Sea region are characterized by stronger southeasterly wind stress anomalies, with clockwise (upwelling) curl northeast of the Solomon Islands where the wind stress anomalies turn westerly (Kessler and Cravatte, 2013). During Pandora, winds were strongly southeasterly (**Figure 4a**), with July corresponding to the height of the southeast trade season. The warmest recordings of sea surface temperature (SST) during Pandora were largely confined equatorward and east of the Solomon Islands, with cooler waters within the Solomon Sea and south toward the winter hemisphere (**Figure 4a**). In contrast, regional winds were extremely weak during MoorSPICE (**Figure 4b**), in keeping with the expected change in the seasonal cycle, but also the coinciding transition from a cold phase to a warm phase of ENSO. During MoorSPICE, SST was largely above 29°C in most of the Solomon Sea. The warmest waters were found in the tropics east of the Solomon Islands, and likely reflected the eastward shift of the western Pacific warm pool in response to westerly wind bursts earlier in the year associated with the El Niño conditions that ultimately failed to materialize (Menkes et al., 2014; McPhaden et al., 2015). Thus, Solomon Sea SST

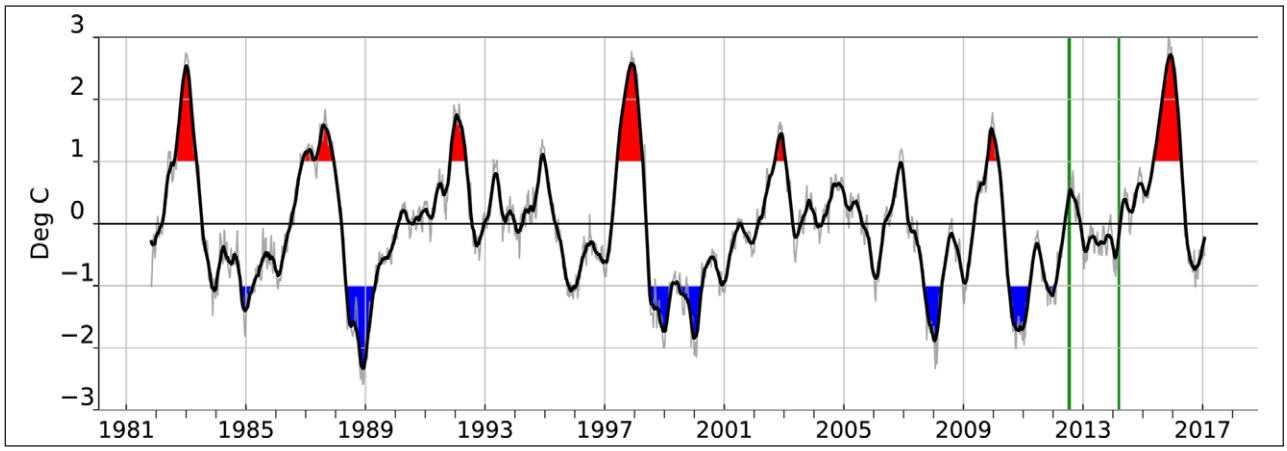

Figure 3: The Niño3.4 sea surface temperature anomaly index from 1982 through January 2017. The relevant region is bounded by 90°W–150°W and 5°S–5°N. The anomaly index (grey line, from http://www.esrl.noaa.gov/psd) is overlaid by a 3-month moving average (black line), where red and blue shading indicate El Niños (Niño3.4 anomalies greater than +1) and La Niñas (Niño3.4 anomalies less than −1), respectively. Green lines indicate the dates of the Pandora (July—August 2012) and MoorSPICE (March 2014) cruises. DOI: https://doi.org/10.1525/elementa.221.f3

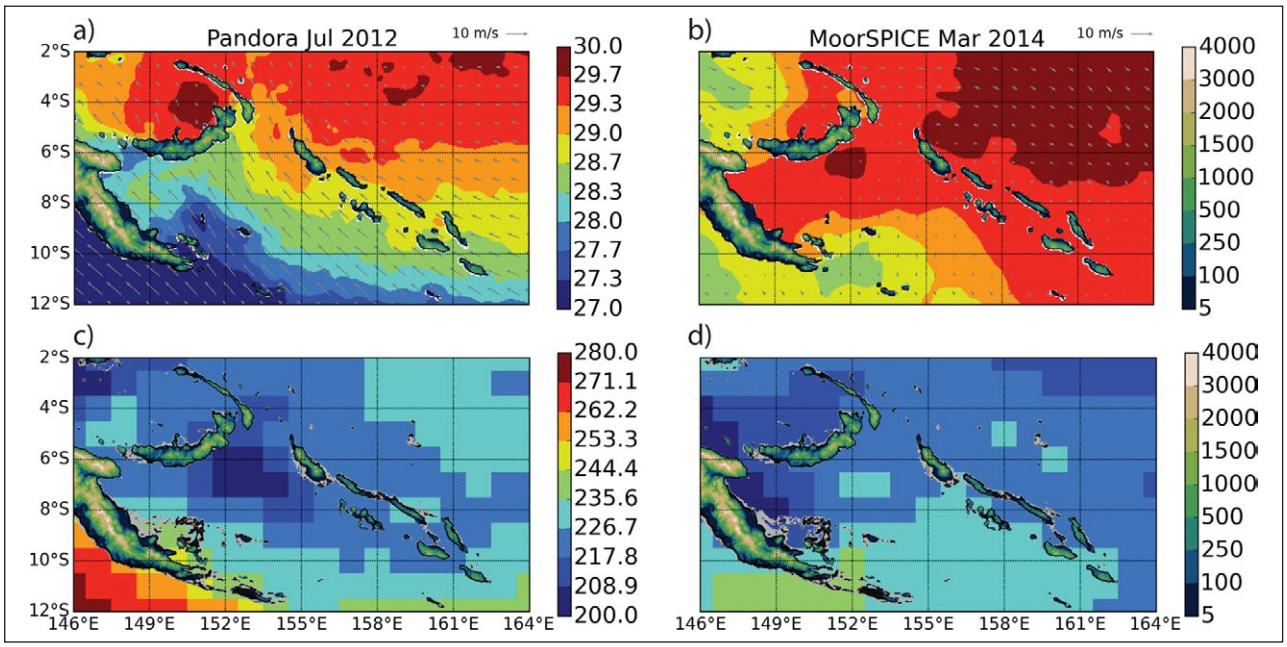

Figure 4: Sea surface temperature, wind vectors and outgoing longwave radiation during the two cruise periods. Data for sea surface temperature (SST in °C, color scale) from the Operational Sea Surface Temperature and Sea Ice Analysis are overlain by ASCAT wind vectors (m s^{-1}) averaged over **(a)** Pandora and **(b)** MoorSPICE cruise periods. Data available from http://marine.copernicus.eu. Unit wind vector is found in the upper right. Outgoing Longwave Radiation (OLR in W m^{-2}, color scale, from http://www.esrl.noaa.gov/psd (Lee, 2014)) also averaged over **(c)** Pandora and **(d)** MoorSPICE cruise periods. Topography is indicated by the colorbar to the right (meters). DOI: https://doi.org/10.1525/elementa.221.f4

and wind patterns are tied to the regional scale seasonal cycle as can be visualized in **Figure 4**.

On intraseasonal time scales, the air-sea coupling of the western Pacific is influenced by the Madden-Julian Oscillation (MJO), a system of large-scale coupled patterns of atmospheric convection and winds that propagate eastward along the equator (Madden and Julian, 1972). An active MJO is characterized by deep convective anomalies that can block the incoming solar radiation and produce anomalously cool SST. The Wheeler and Hendon (2004) index breaks the MJO cycle into eight phases that correspond to the shifting location of the maximum intraseasonal winds and convection (derived from satellite measurements of outgoing longwave radiation (OLR, W m^{-2}). During Pandora, MJO anomalies based on the Wheeler and Hendon Index suggest an extremely weak active phase of the MJO, while for MoorSPICE, MJO activity was strong in late February, just before the cruise (not shown).

These stable conditions suggest that at least during the time of the cruises, MJO and intraseasonal wind forcing did

not likely play a strong role in upper ocean variability or circulation. However, the apparent weak variability during both cruises was fortuitous since four anticyclones migrated south of 10°S during Pandora, nevertheless leaving near stationary conditions over the Solomon Sea. Atmospheric conditions were more unstable during MoorSPICE, promoting the formation of tropical cyclones (TC): weak TC HADI (Category 1, March 9–11 south of 10°S) and severe TC LUSI (Category 3, March 9–16, over the north Vanuatu Islands). A third TC (GILLIAN, March 21–26) formed in the Southwest Pacific too, but just outside the Solomon Sea (http://www.bom.gov.au). In the end, none of these TCs directly impacted oceanic conditions in the Solomon Sea during the cruise time of MoorSPICE.

Similar OLR values of around 220–230 W m^{-2} were found during both Pandora (**Figure 4c**) and MoorSPICE (**Figure 4d**). Low OLR (cloudier) was mostly confined north of the equator during Pandora, probably indicating the location of the western Pacific Intertropical Convergence Zone. During MoorSPICE, the minimum in OLR to the east of the Solomon Sea indicates the equatorward axis of the South Pacific Convergence Zone (SPCZ), which is more active during the Southern Hemisphere summer.

The July–August 2012 cruise conditions were therefore mainly representative of the strong-trade wind season, while the March 2014 cruise conditions were representative of the opposite weak-trade wind season. Interannual and intraseasonal variability are not expected to be of major influence.

Results

Sea surface temperature and salinity

The sea surface conditions during both cruises were assessed using the along-track direct measurements of in situ winds, sea surface salinity (SSS) and SST (Table S1; **Figures 5** and S3 for complete cruise track). During Pandora, we observed strong (~20 m s^{-1}) and unidirectional winds oriented equatorward along the prevalent trade wind axis (**Figure 5a**). During MoorSPICE winds were much weaker (~5 m s^{-1}) along an identical axis and were poleward to the north of 6°S and equatorward to the south of this latitude (**Figure 5b**). In situ winds (**Figure 5**) agree well with the monthly mean satellite winds (**Figure 4**) for both cruises.

Sea surface waters in the Solomon Sea appeared to be saltier and colder during Pandora compared to MoorSPICE (**Figure 5**) except northeast of Bougainville Island. The SSS was dominated by small scale gradients during Pandora, while during MoorSPICE salinity features were much more cohesive on a large scale, especially within the northern exit straits of the Solomon Sea. The SST exhibited a stronger zonal cross-basin gradient during Pandora compared to MoorSPICE, with lower temperature on the western part of the Solomon Sea (**Figure 5c, d**). Similar patterns were found in the monthly mean satellite SST for both cruises (**Figure 4a, b**), consistent in SST and SSS seasonal variability described in Delcroix et al. (2014). These colder and saltier waters are due to northwestward oceanic advection (**Figures 5**, S3).

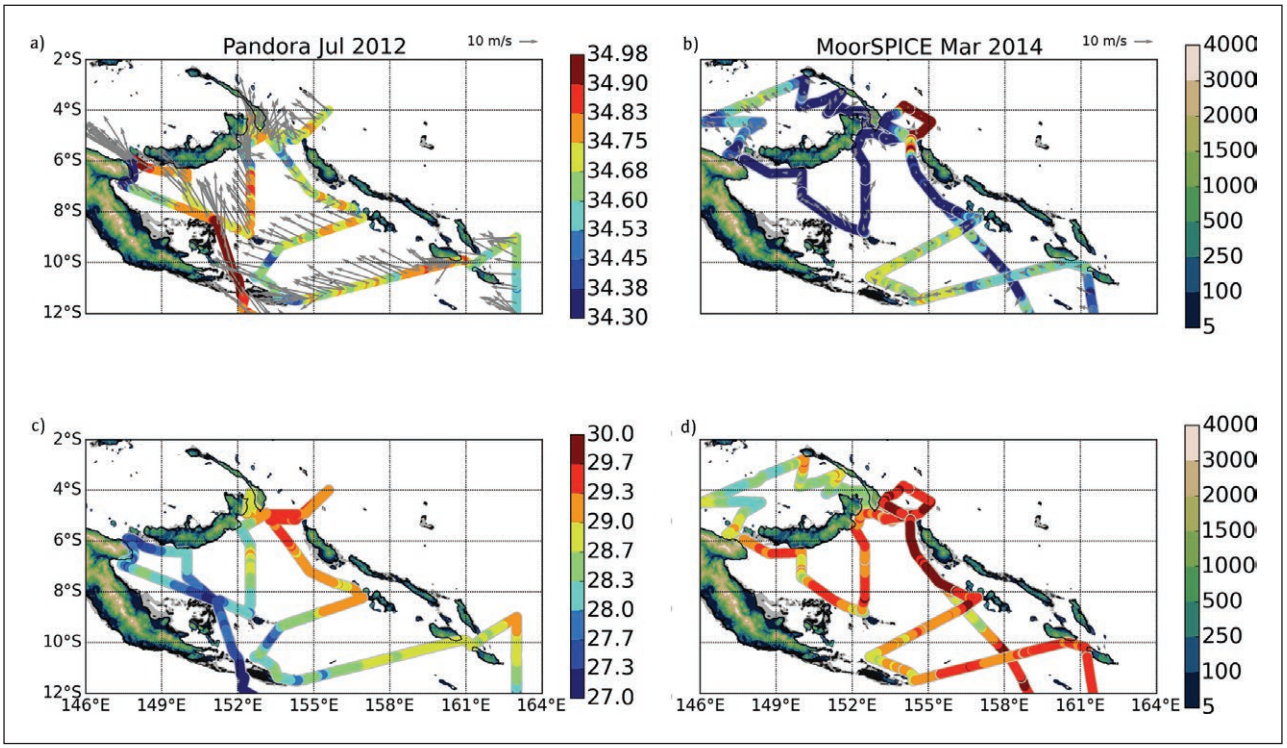

Figure 5: Observed along-track surface salinity, winds and temperature. In situ measurement of salinity (color scale) is plotted along with winds (in m s^{-1}, unit wind vector is found in the upper right) during **(a)** Pandora and **(b)** MoorSPICE, along with along-track sea surface temperature (°C, color scale) during **(c)** Pandora and **(d)** MoorSPICE. Topography is indicated by the colorbar to the right (meters). DOI: https://doi.org/10.1525/elementa.221.f5

Volcanic influences

Results of the pH survey are displayed in **Figure 6a**. The atmospheric transport and dispersion of acidic species released from Rabaul, Bagana and Ambrym volcanoes were forecast onboard using the atmospheric circulation model WRF-Flexpart (Mari et al., 2014; Lefevre et al., 2015) (**Figure 6b**). Cloud waters in the pristine marine boundary layer are characterized by pH values ranging from 6 to 7, but large pH decreases of 1 to 2 units were recorded in cloud waters contaminated by the volcanic plumes. A very acidic rainfall (pH = 4.1) was found >500 km downwind of Ambrym volcano (3 July 2012). The volcanic source of acidifiers was confirmed by air trajectory results (**Figure 6b**). Six days later (9 July 2012), the volcanic plume had crossed over the Louisiades archipelago (**Figure 1**), more than 1000 km

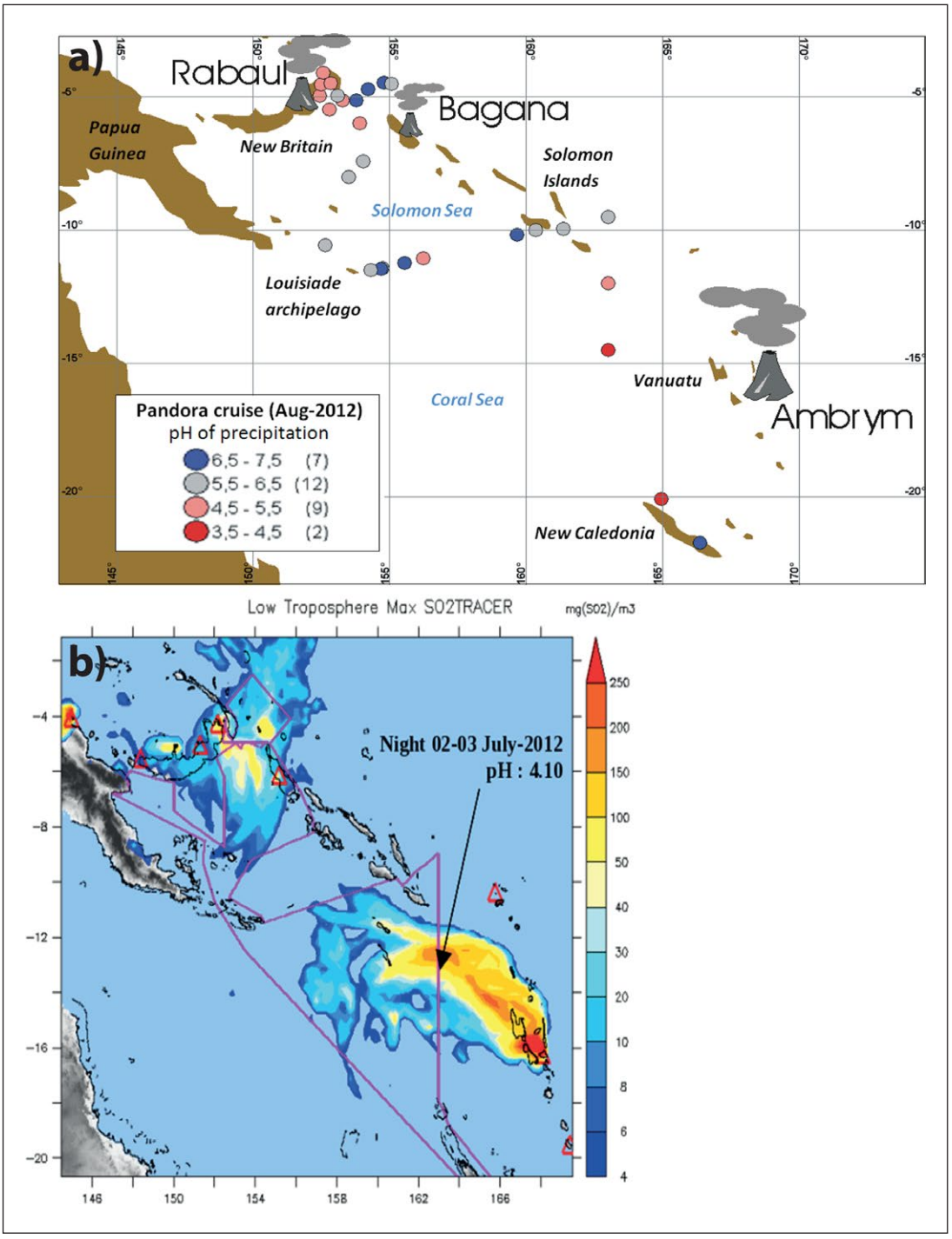

Figure 6: Volcanic impact on atmospheric conditions. (a) Distribution of pH in rainwater during the Pandora cruise, with main volcanic SO_2 emitters superimposed. Color indicates Ph; the number of occurrences in the color range is indicated in parenthesis. **(b)** Example of the simulated volcanic plume dispersion (here SO_2 is used as tracer) for the night 2–3 July 2012 using the atmospheric model WRF-Flexpart. The Pandora cruise track is in magenta; color scale indicates the simulated sulfur concentration. DOI: https://doi.org/10.1525/elementa.221.f6

away from Ambrym volcano acid rain with a collected pH of 5.4.

The presence of volcanogenic acidifiers is explained by the long range transport of sulfate precursors from Ambrym discussed in Lefevre et al. (2015): from July 5–15. A strong anticyclone (1030 hPa) in the northern Tasman Sea (http://www.bom.gov.au) drove a rapid and steady southeasterly trade wind flux, promoting the transport of volcanogenic acid species from Ambrym to the sampling site within a couple of days.

It is worth noting that close to Rabaul volcano, cloud chemistry is also influenced by local magma degassing (**Figure 6b**). Finally, the pH distribution (**Figure 6a**) is in good agreement with the mean distribution of surface sulfate concentrations and total sulfate (dry + wet) flux deposition displayed in Lefevre et al. (2015, their **Figure 13a, b**).

Ocean circulation

The observed currents were generally strong with high energy at mesoscale (~100 km) and submesoscale (~10 km) so that snapshots from each cruise contain variability on many time scales. Currents derived from satellite altimetry and drifters suggest that the mean surface circulation during Pandora was dominated by a westward flow in most of the Solomon Sea (**Figure 7a**). The shipboard ADCP shows a strong and narrow NGCU entering the Solomon Sea (**Figure 7c**). The NGCU core is located between 500 and 1000 m depth with a surface reversal above 100 m (Germineaud et al., 2016, Figure S4a), as also observed by repeated glider transects (Davis et al., 2012).

As the NGCU splits around Woodlark Island, a strong, shallower stream traveled to the west through the Milne Bay, while the other stream was eastward, and stronger below 100 m (153.5°E, 9°S; **Figure 7c**). This asymmetry is likely due to the sill depth of the passage between Woodlark Island and Trobriand (151.5°E, 8.5°S) which is about 350 m (Figure S4a). A moderate (~0.5 m s^{-1}) surface-enhanced flow was observed entering the Solomon Sea through the very narrow Indispensable Strait (**Figure 7c**). The portion of the NGCU that exited the Solomon Sea through Vitiaz Strait was strong (>1 m s^{-1}) over the full depth (Germineaud et al., 2016).

While the bifurcation of the NGCU south of New Britain was not sampled, the resulting NBCU was captured at 152°E with flow along the coast to the northeast at all depths and a portion exiting through St. Georges Channel with the current's core between 100 and 400 m depth (Germineaud et al., 2016, **Figure 7c**). The circulation at Solomon Strait was stronger near the coast of New Ireland and northward below 100 m as the southward flow was

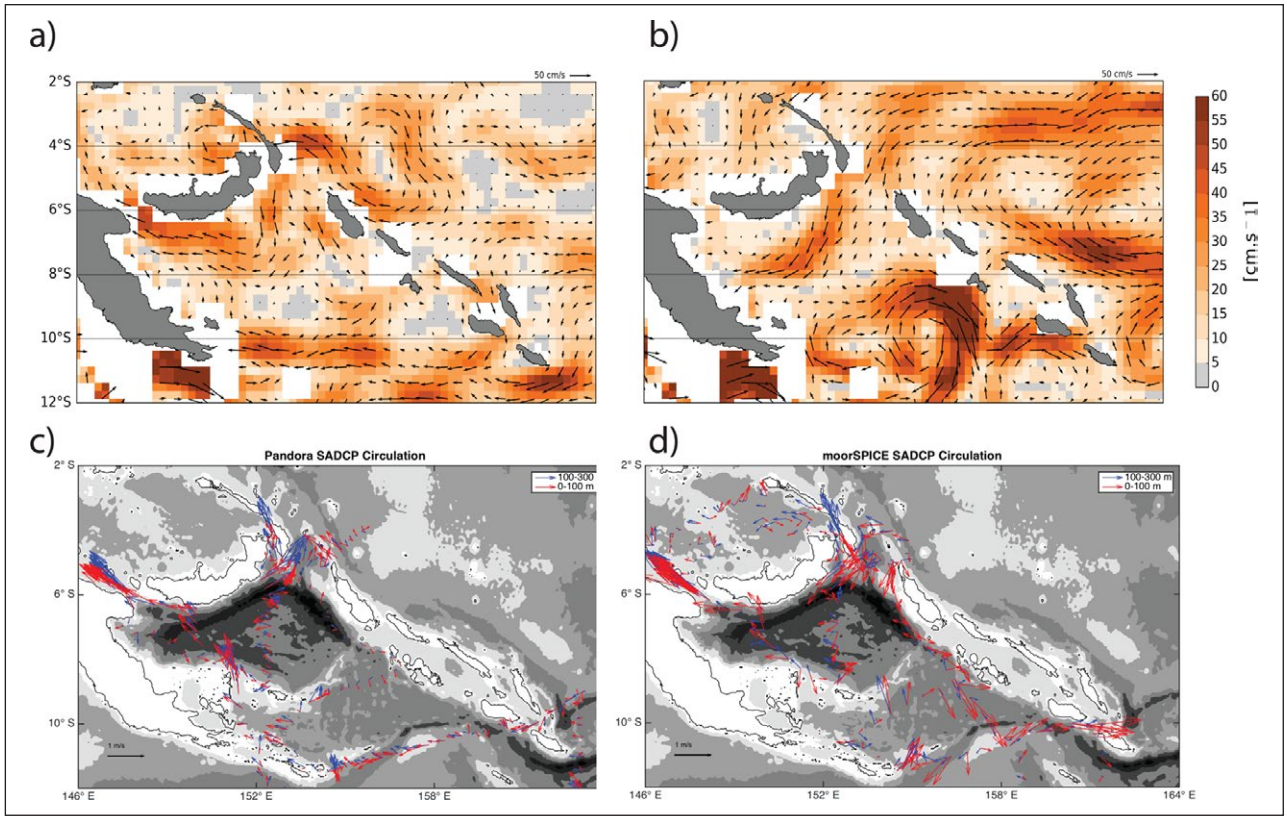

Figure 7: Surface currents. Geostrophic surface velocity anomalies derived from satellite altimetry (AVISO-DUACS14) during **(a)** Pandora (average July–August 2012) and **(b)** MoorSPICE (average March 2014) combined with the annual mean surface current climatology from the global drifter program (GDP, 1979 through March 2015) (from http://www.aoml.noaa.gov/phod/dac/dacdata.php). Underway currents from the S-ADCP in the layers 0–100 m (red) and 100–300 m (blue) during **(c)** Pandora and **(d)** MoorSPICE. Unit current vectors are found in the upper right corners.
DOI: https://doi.org/10.1525/elementa.221.f7

confined to the upper 100 m and to the western half of the Solomon Strait (**Figure 7c**).

East of Solomon Islands and south of 6°S (**Figure 7a**), there is a branch of the westward SEC with an eastward current to the north (2°–6°S). Cyclonic circulations occur South of Papua New Guinea (11°S, 148°E) and northeast of Bougainville Island (5°S, 156°E) (**Figure 7a**). This last feature is related to a strong northwestward surface flow along the east coast of Bougainville Island (155°E, 5°S; **Figure 7c**).

During MoorSPICE the surface circulation was dominated by cyclonic eddies at the southern entrance of the Solomon Sea (**Figure 7b**). The current was southward through Solomon Strait, contributing to a large anti-cyclonic eddy inside the Solomon Sea (8°S, 153°E). East of Solomon Islands, the flow was eastward at 8°S, that is, against the time-mean flow in the SEC with large eddies centered at 6°S and 10°S.

Compared to during the Pandora cruise, the NGCU was shallower and wider during MoorSPICE, with no surface reversal as it entered the Solomon Sea (Germineaud et al., 2016, **Figures 7d**, S4b). No NGCU bifurcation around Woodlark Island was observed during MoorSPICE, with eastward flow east of Milne Bay, that is, opposite to the direction found during Pandora.

This contrast was also observed in drifter climatology during this season (Hristova and Kessler, 2012). However the merging of a very strong and deep NGCU was observed north of the Woodlark Island chain. The outflow through Vitiaz Strait was unexpectedly strong (>1 m s^{-1}), and so not consistent with the expected seasonal decrease. Nevertheless, the flow decreases with depth, and the total transport through Vitiaz Strait was much lower (Germineaud et al., 2016). The NBCU had a similar speed and direction to that found during Pandora. Surface flow (0–100 m) in both St. Georges Channel and Solomon Strait was entirely southward into the Solomon Sea, then to the southwest along the coast of New Britain.

In addition, strong variations in spatial mixing patterns were also detected between both cruises. Observations from the Pandora and MoorSPICE cruises and the Argo database were used to estimate the dissipation of kinetic energy and mixing in the Solomon Sea using the Thorpe scale method and finescale parametrization (Alberty et al., 2017). The mean profile of dissipation in the Solomon Sea provided in that work shows that the maximum is near the surface and decreases with depth. Depth-mean dissipation in the Solomon Sea was elevated by a factor of 8 relative to the rest of the equatorial Pacific and spatial patterns of mixing vary by up to two orders of magnitude along isopycnal layers. The results suggest seasonal variability of mixing with enhancement during strong monsoonal winds, though the full seasonal cycle remains unresolved.

The two cruises therefore show contrasted circulations, which we attribute to the expected seasonal variability as both the intraseasonal and interannual contrasts are low between the two cruises (Section on Climatic Context). Pandora was characterized by strong and well defined currents that are typical of austral winter (e.g., Cravatte et al., 2011; Hristova and Kessler, 2012), while MoorSPICE was characterized by weaker currents and a greater activity of cyclonic eddies, typical of early austral summer (Gourdeau et al., 2014; Hristova et al., 2014).

Water properties

Germineaud et al. (2016) provide a detailed analysis of thermocline and intermediate water properties and we summarize here the main features. Near the surface, water properties have an essentially homogeneous salinity during Pandora (34.4–35.4; **Figure 8a**) and a large range during MoorSPICE (33.2–35.6; **Figure 8b**).

Below the surface, water masses are identified by marked temperature and salinity extremes. During Pandora, salinities reach a maximum around 200 m depth (>35.8) at σ_θ = 24.5 (**Figure 8a**) characterizing the South Pacific Tropical Water (SPTW, Wyrtki, 1962), also referred as the *Upper Salinity Maximum* with south/east Pacific origins (Donguy 1994; Qu and Lindstrom, 2002). This upper salinity maximum was found at $\sigma_\theta \sim 25$ during MoorSPICE with salinities (<36) lower than during Pandora (**Figure 8b**).

Below the SPTW is the Subtropical Mode Water (STMW; σ_θ = 25 – 26.5 kg m^{-3}, 12°–20°C) coming from the northern part of the Tasman Sea (Donguy and Henin, 1977; Holbrook and Maharaj, 2008). Deeper, waters in the density range close to σ_θ = 27.0 kg m^{-3} (5°–8°C, **Figure 8a**) indicate the Subantarctic Mode Water (SAMW; McCartney, 1977) formed at the northern edge of the Antarctic Circumpolar Current south of Tasmania and then advected northward into the South Pacific (e.g., Grenier et al., 2013; Kessler and Cravatte, 2013).

Near 800 m depth at σ_θ = 27.2 kg m^{-3}, a salinity minimum (<34.6) associated with a maximum in oxygen content (~150–200 μmol kg^{-1}; **Figure 8a**) identifies the Antarctic Intermediate Water (AAIW) that originates in the southeast Pacific (Qu and Lindstrom, 2004). AAIW is also associated with marked increases in silicate (**Figure 8c, d**) and nitrate (**Figure 8e, f**) observed below $\sigma_\theta \sim 27$. Northeast of Bougainville Island (~5°S–155°E; Figure S9), the highest salinities of the intermediate waters indicate the presence of the South Equatorial Pacific Intermediate water (SEqPIW that emanates from the equatorial region, Bostock et al., 2010; Germineaud et al., 2016).

An increase in salinity at σ_θ = 27.4 (>1000 m) associated with high nutrient content characterizes the Upper Circumpolar Deep Water (UCDW), which is consistent with Sokolov and Rintoul (2000, their **Figure 12b**). We observed quite low oxygen content associated with high concentrations in nitrate (>30 μmol kg^{-1}) and silicate (>100 μmol kg^{-1}), with high salinity (>34.5) during both cruises. The UCDW emanates southeast of New Zealand, before reaching the anticyclonic gyre in the South Pacific (Tsimplis et al., 1998; Kawabe and Fujio, 2010).

Below, the major deep and bottom waters are characterized by the Lower Circumpolar Deep Water (LCDW), which corresponds to an increase in salinity and a decrease in silicate near 2000 m in the Southern Ocean (Orsi et al., 1999). This deep water flows northward across the Southwest Pacific via complex pathways (Kawabe and

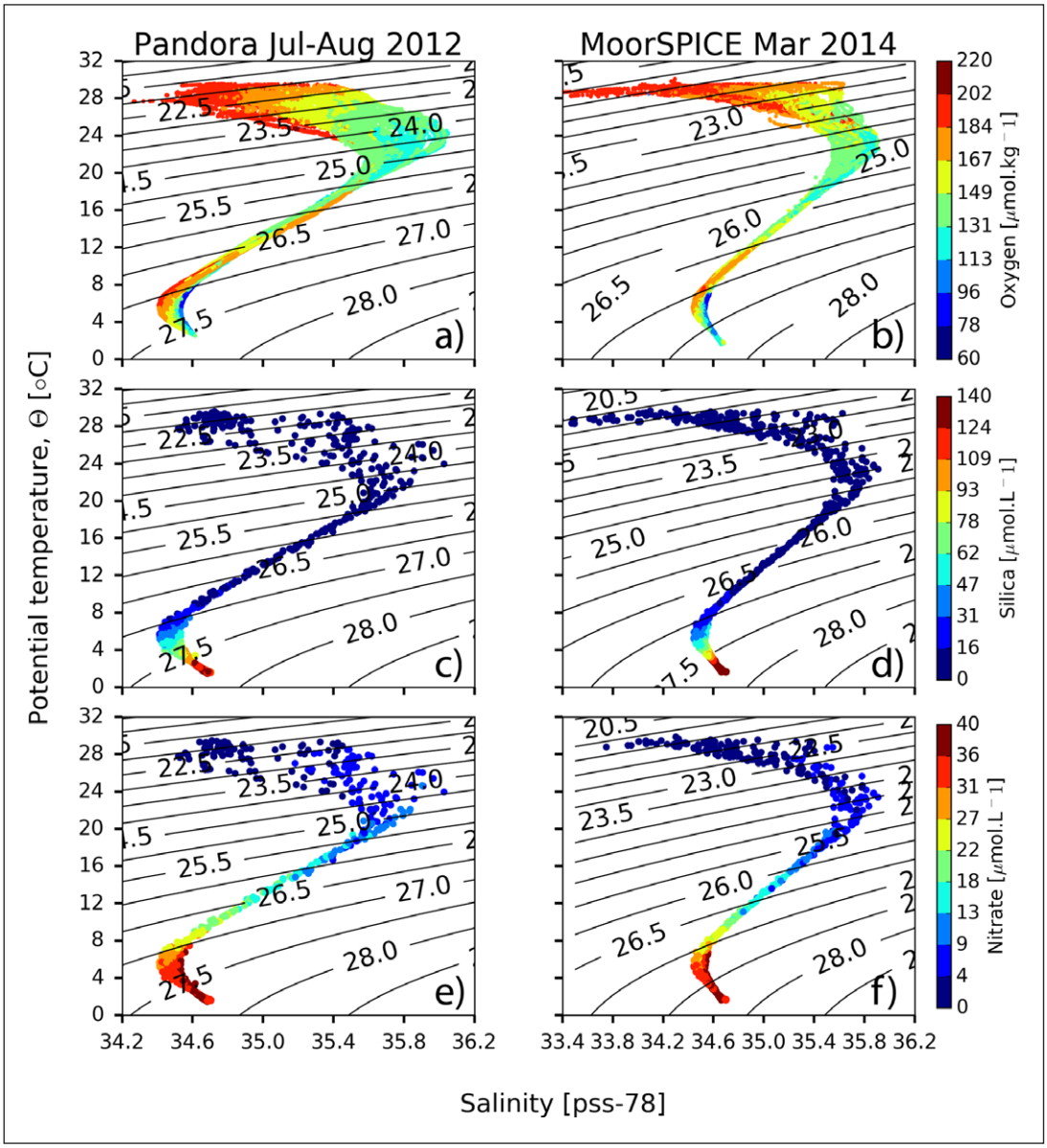

Figure 8: Water mass properties. (Left) Pandora; (right) MoorSPICE color-coded by oxygen **(a, b)**; silicate **(c, d)**; nitrate concentration **(e, f)**. Iso-contours indicate potential density. DOI: https://doi.org/10.1525/elementa.221.f8

Fujio, 2010, their **Figure 2c**), although its presence within the Coral and Solomon Seas remains poorly documented.

N_2 fixation, primary production and diazotroph abundances

Bonnet et al. (2015) and Berthelot et al. (2017) have provided a detailed quantification of N_2 fixation and diazotrophs in the Solomon Sea; here we summarize here the main results and trends. In general, *Trichodesmium* dominated the diazotroph community in the Solomon Sea with up to 8.2×10^{10} *nifH* copies m^{-2} during Pandora and up to 4.8×10^{9} *nifH* copies m^{-2} during MoorSPICE (**Figure 9a**) (Bonnet et al., 2015). These abundances are in the upper range of *nifH*-derived *Trichodesmium* abundances in the world ocean (Luo et al., 2012). UCYN were the second most abundant phylotypes during Pandora (average of 4.0×10^{9} *nifH* copies m^{-2}; **Figure 9**). Maxima were observed at the centre of the Solomon Sea (8.0×10^{9} *nifH* copies m^{-2}) during MoorSPICE, with much lower maximum abundances in the Bismarck Sea ($<1.3 \times 10^{8}$ *nifH* copies m^{-2}) (**Figure 9b**). *Trichodesmium* dominates over UCYN phylotypes in the Solomon Sea in contrast with other South Pacific areas such as the Coral Sea. This dominance seems to be associated with the meridional temperature gradient between the Solomon and the Coral Sea, as well as the higher trace metal availability in the Solomon Sea (Section on geochemistry, Moisander et al., 2010; Bonnet et al., 2015).

In the Solomon Sea, photic N_2 fixation rates ranged from 30 to 5449 (average 624) μmol N m^{-2} d^{-1} during Pandora and 0.2 to 4364 (average 1396) μmol N m^{-2} d^{-1} during MoorSPICE (**Figure 9c**). They were significantly higher during austral summer conditions (MoorSPICE) than during austral winter conditions (Pandora), suggesting a possible seasonal effect. Nonetheless, rates during both seasons were in the upper range of those reported in the global N_2

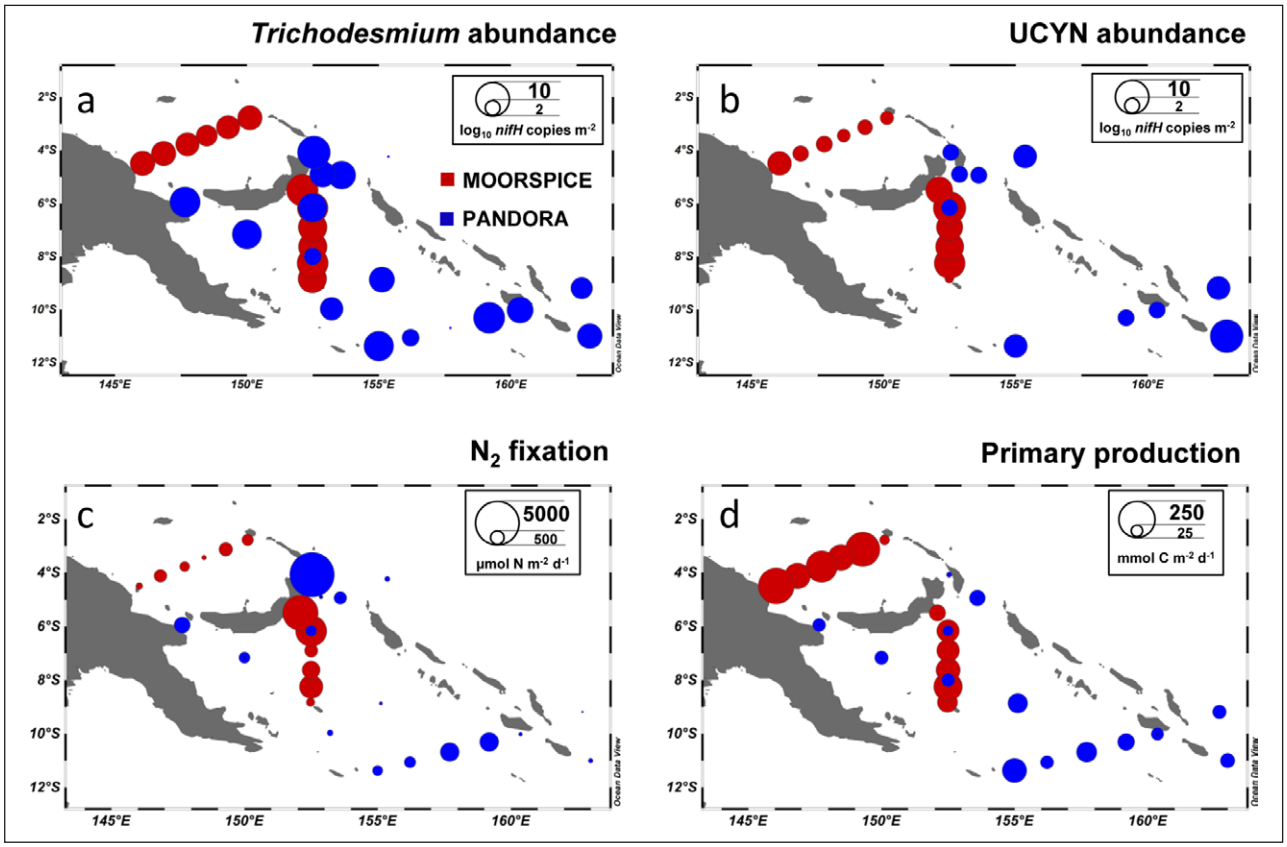

Figure 9: Nitrate fixation. (a) *Trichodesmium* and **(b)** UCYN abundances (log *nifH* copies m^{-2}), **(c)** N_2 fixation rates (μmol N m^{-2} d^{-1}), and **(d)** primary production rates (mmol C m^{-2} d^{-1}), during the Pandora (austral winter, blue dots) and MoorSPICE (austral summer, red dots) cruises. All data are integrated over the 0–100 m layer, corresponding approximately to the photic zone. DOI: https://doi.org/10.1525/elementa.221.f9

fixation MAREDAT database and even surpassed its upper rates (100–1000 μmol N m^{-2} d^{-1}). This comparison suggests that the Solomon Sea is a hot spot of N_2 fixation in the global ocean, although the reasons behind these high rates need to be further investigated. We hypothesize that having SST values >27°C all year round (i.e., optimal for diazotrophic growth and nitrogenase activity, Breitbarth et al., 2007) associated with significant micro- and macronutrient inputs provide ideal conditions for N_2 fixation. In particular, phosphate turnover times have been reported to be >2 days (i.e., non-limiting for phytoplankton communities) further south around Melanesian archipelagoes (Moutin et al., 2005), which is likely the case in the Solomon Sea as surface phosphate concentrations were never exhausted during both cruises (always >0.08 μmol L^{-1}).

In addition, iron, an important component of the nitrogenase enzyme which catalyzes N_2 fixation (Raven, 1988), is continuously provided to the Solomon Sea through land runoff, hydrothermal, and volcanic activity (see section Dissolved Iron below and Labatut et al., 2014) and possibly through energetic currents interacting with the islands (Grenier et al., 2013; 2014; Djath et al., 2014). The dissolved Fe measurements performed along a west–east zonal section in the equatorial Pacific (Slemons et al., 2010) confirm that the Solomon Sea is a primary source of iron for the equatorial Pacific.

Altogether, these conditions provide optimal environmental conditions for diazotrophs to bloom extensively and likely explain why this regional sea is a hot spot of N_2 fixation. The basin-scale South Pacific N_2 fixation rate was estimated at 46 Tg N y^{-1} (Luo et al., 2012), equivalent to a daily water column integrated rate of 125 μmol N m^{-2} d^{-1} (considering an area of 72 × 10^6 km^2 for the South Pacific). The N_2 fixation rates measured during the Pandora and MoorSPICE cruises are larger by a factor of 7 (529 μmol N m^{-2} d^{-1} on average and up to >5000 μmol N m^{-2} d^{-1}; **Figure 9c**), confirming that the Solomon Sea contributes importantly to fixed nitrogen inputs in the South Pacific as a whole.

In an attempt to assess the importance of N_2 fixation in this region, we extended the depth-integrated N_2 fixation rates obtained during both cruises to the Solomon Sea surface (7.2 × 1011 m^2). Assuming that diazotrophs fix on average 600 μmol N m^{-2} d^{-1} during the austral winter conditions (Pandora) and 1300 μmol N m^{-2} d^{-1} during austral summer conditions (MoorSPICE), N_2 fixation would introduce 3.5 Tg N y^{-1} to the Solomon Sea. This amount corresponds to ~10% of the total nitrogen fixed for the entire South Pacific Ocean as reported in Luo et al. (2012), while the Solomon Sea represents only 1% of its total area. Consequently, the N_2 fixation budget for the South Pacific needs to be updated by including these recent studies performed in the Solomon Sea.

The nitrogen demand derived from primary production data (**Figure 9**) (assuming a C:N ratio of 6.6) indicates

that N_2 fixation fueled on average 5.5 and 15.1% of total primary production in the Solomon Sea during the Pandora and MoorSPICE cruises, respectively. This contribution is remarkably high compared to other oceanic regions such as the Northwestern Pacific (Shiozaki et al., 2013), Southeastern Pacific (Raimbault and Garcia, 2008), Northeast Atlantic (Benavides et al., 2013) or the Mediterranean Sea (Bonnet et al., 2011; Ridame et al., 2014), where the contribution of N_2 fixation to primary production is generally <5%. These higher contributions confirm the importance of N_2 fixation in supplying new nitrogen to the surface waters of the Solomon Sea.

By using high-resolution nanometer scale secondary ion mass spectrometry (nanoSIMS) coupled with $^{15}N_2$ isotopic labelling and flow cytometry cell sorting, Bonnet et al. (2016) showed during MoorSPICE that 10% of diazotroph-derived N was quickly (48 h) transferred to non-diazotrophic plankton, in particular diatoms, whose abundance increased 3-fold in that time frame. Diatoms are efficient carbon exporters to depth (Nelson et al., 1995), suggesting that N_2 fixation may sustain an indirect export pathway of organic matter in the Solomon Sea. It would be interesting in further studies to quantify the part of exported material sustained by diazotrophy in such a hot spot of N_2 fixation.

Inorganic carbon observations, anthropogenic CO_2 and acidification

Although during Pandora samples were taken at contrasted locations, depth profiles for both TA and DIC were relatively depth-independent below 2000 m, as compared to surface gradients (**Figure 10a, b**). Below the surface, a pronounced TA subsurface maximum around 150 m was clearly recognized in the SPTW (**Figure 8**). In intermediate waters (500–1000 m), TA and DIC regularly increased with depth.

However, at station 44 (4°S–155°E, i.e. outside the Solomon Sea in the western tropical Pacific) we observed localized DIC maxima around 500–700 m (highlighted in **Figure 10b**) in the core of the low oxygen layer characterizing old SEqPIW of northern origins (Section on water properties). In deep waters (>1000 m) DIC and TA concentrations presented, like nutrients, a maximum around 2000–3000 m. However, lower DIC and TA concentrations (highlighted in **Figure 10a, b**) were found around 3000 m at station 29 (11°S, 156°E) associated with lower nutrient concentrations, high salinity and high oxygen (11.5°S, 155.7°E).

In surface waters, the range for TA (2270–2290 μmol kg^{-1}), for DIC (1920–1955 μmol kg^{-1}), for pH (8.06–8.09) and for Aragonite saturation state (3.8–4) are typical values observed in the eastern Indian and western Pacific tropical zones (Takahashi et al., 2014; Lenton et al., 2016). Sea surface fCO_2 (calculated) was around 350 μatm at 14°S–162°E and higher at 370 μatm around 4°S–152°E, a difference that could be explained by warming in the north. The fCO_2 range derived from surface DIC/TA data is coherent with underway fCO_2 measurements conducted in this region during July–August 2012 (Trans–Future 5 cruise reported on **Figure 11**, available on SOCAT-V3 data-base, online at www.socat.info, Bakker et al., 2016).

In July 2012 the global mean atmospheric concentration was about 392 ppm (or 378 μatm when converting to fCO_2) (Le Quéré et al., 2015) Therefore, during the cruise the region was a CO_2 sink (oceanic fCO_2 was lower than in the air). To understand how the oceanic carbon uptake propagates in the water column,

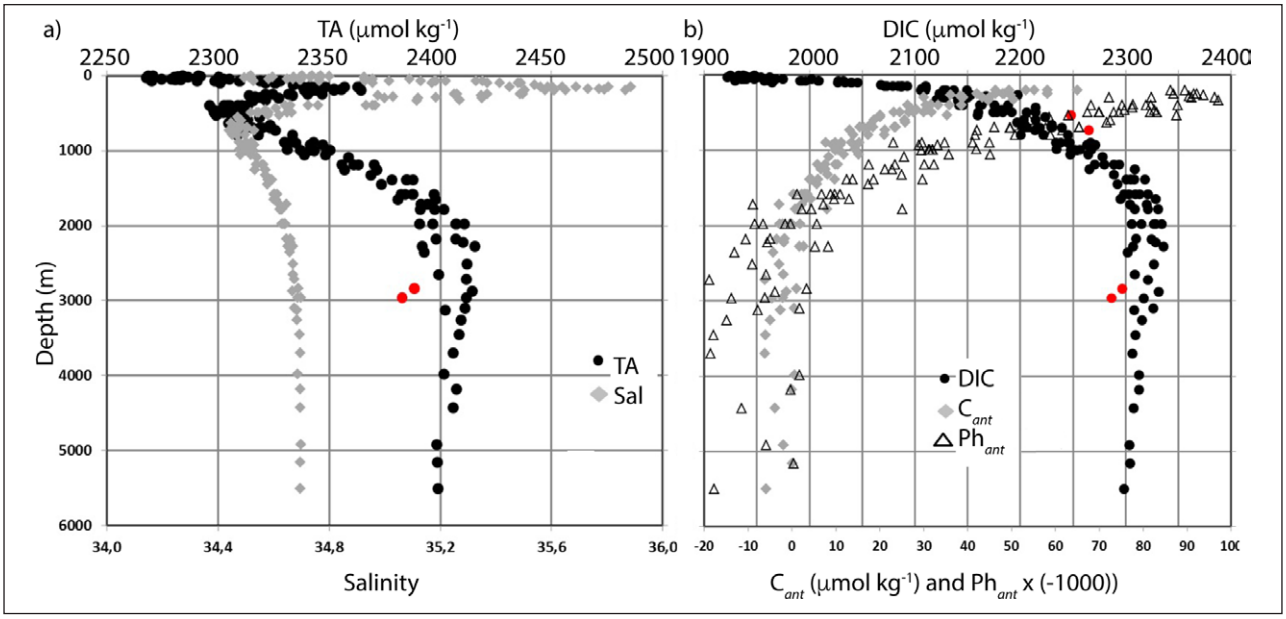

Figure 10: Inorganic carbon observations, anthropogenic CO_2 and acidification during Pandora. (a) Salinity (grey) and TA (black) (μmol kg^{-1}) profiles; **(b)** DIC (black, μmol kg^{-1}), C_{ant} (grey, μmol kg^{-1}) and pH_{ant} profiles (triangles). For scaling purpose in (b), pH_{ant} values are multiplied by −1000 (i.e., 100 = −0.1 unit pH change). In (a) and (b) red dots highlight anomalies observed at a few locations. Uncertainty on C_{ant} estimate is about ±7 μmol kg^{-1}. DOI: https://doi.org/10.1525/elementa.221.f10

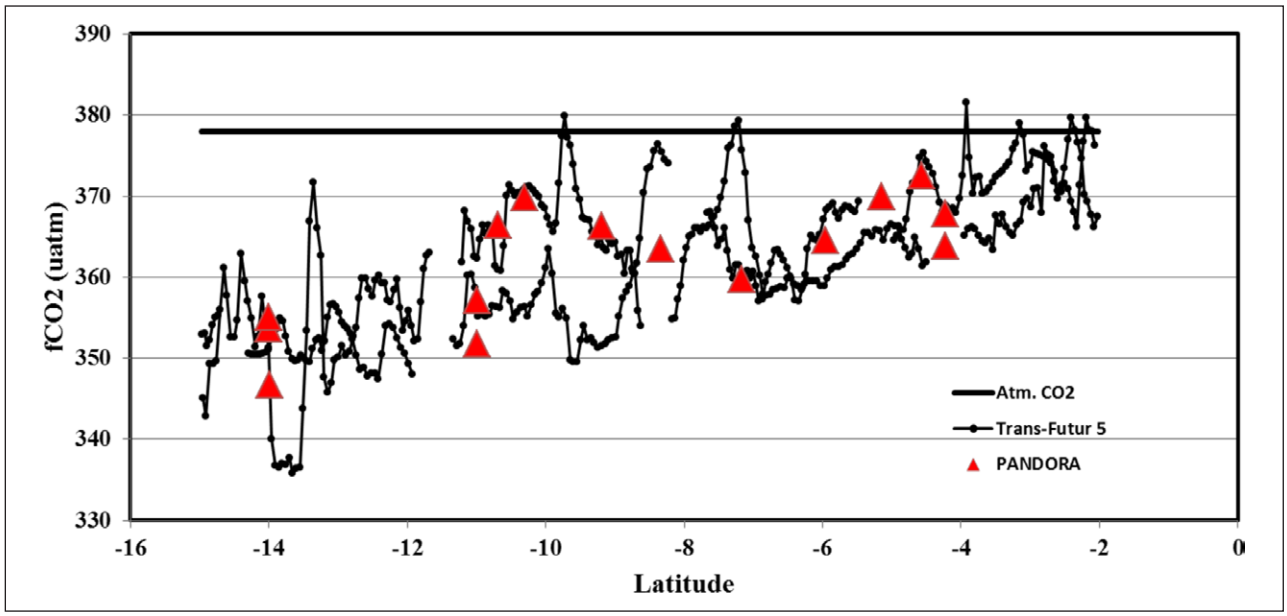

Figure 11: Sea surface fCO_2. Pandora values are calculated with DIC/TA (red triangles); Trans-Future cruise data in July–August 2012 are from underway fCO_2 measurements (black dots) in North Coral Sea and Solomon Sea from SOCAT-V3 (Bakker et al., 2016). Both observations show lower sea surface fCO_2 compared to atmospheric fCO_2 (black line). During this period, the region was a CO_2 sink. DOI: https://doi.org/10.1525/elementa.221.f11

we evaluated the anthropogenic CO_2 concentrations (C_{ant}) using the method based on the TrOCA tracer (a combination of TA/DIC pairs, temperature, salinity and oxygen data) previously applied in the Indian Ocean along several WOCE sections (Touratier et al., 2007; Alvarez et al., 2009). The new TrOCA method proposed by Touratier et al. (2007) was considered the most suitable for the investigated region because no transient tracers (e.g., CFCs) were measured during the Pandora cruise. The C_{ant} concentrations are presented only below 200 m (**Figure 10b**) as the method is not suitable to evaluate C_{ant} in surface layers.

The C_{ant} vertical gradient suggests a significant penetration of anthropogenic CO_2 down to about 1500 m. Between 200 and 1000 m C_{ant} concentrations decreased sharply from about 50 μmol kg^{-1} to 10 μmol kg^{-1}. Below 1500 m, the C_{ant} concentrations are low and within the error of the method (±7μmol kg^{-1}).

We also estimated the anthropogenic pH_{ant} by calculating the difference between modern pH, (based on DIC and TA concentrations in 2012) and pre-industrial pH values (based on DIC-C_{ant} and TA concentrations). As expected, the pH_{ant} profiles mirror the C_{ant} penetration (**Figure 10b**). A large pH_{ant} value of about –0.1 units is estimated in upper layers (200 m) and is also significant at depth (–0.05 units at 500 m).

The DIC and TA observations obtained during the Pandora cruise enable the first evaluation of both anthropogenic carbon and ocean acidification in the Solomon Sea. Added to historical observations conducted in the Western Tropical Pacific ocean (Suzuki et al., 2013), these data can be used to investigate in more detail the oceanic inorganic carbon system and its variability in a broader context.

Trace elements

We present below an initial examination of the concentration of Fe, Al, Hg and Mn in the Solomon Sea.

Dissolved Iron

Depth profiles of dissolved Fe (dFe) resemble nutrient-like profiles, with low concentrations at the surface and an increase with depth (**Figure 12a**). The surface dFe concentrations ranged from 0.11 to 0.44 nmol L^{-1} (**Figure 12b**) and showed significantly ($p < 0.05$) higher dFe concentrations near the islands (0.35 ± 0.06 nmol L^{-1}) than in the Coral Sea (0.23 ± 0.07 nmol L^{-1}) in the first 150 m. Similar concentrations have been observed by Labatut et al. (2014) off the Papua New Guinea coast due to river runoff. Volcanic inputs from the Rabaul volcano (close to station 42) could also be involved. This enrichment is confined near islands and offshore, dFe concentrations (0.19 ± 0.02 nmol L^{-1}) are not significantly ($p > 0.05$) different from those in the Coral Sea. High primary production and *Trichodesmium* abundance could explain the similar dFe stocks (Bonnet et al., 2015). The deep water dFe concentrations ranged from 0.62 to 1.29 nmol L^{-1} (**Figure 12c**) and suggest a sedimentary and/or hydrothermal source of dFe in the Solomon Strait (Labatut et al., 2014).

Al and Mn

Enrichments in Al and Mn concentrations in the region relative to the open ocean indicate that coastal and sedimentary input is important in this region and that this *boundary exchange* is likely driven by strong currents scouring the coastal margin. However, quantification of boundary exchange requires the coupling of concentrations of rare earth elements (REE) and measurements of Nd

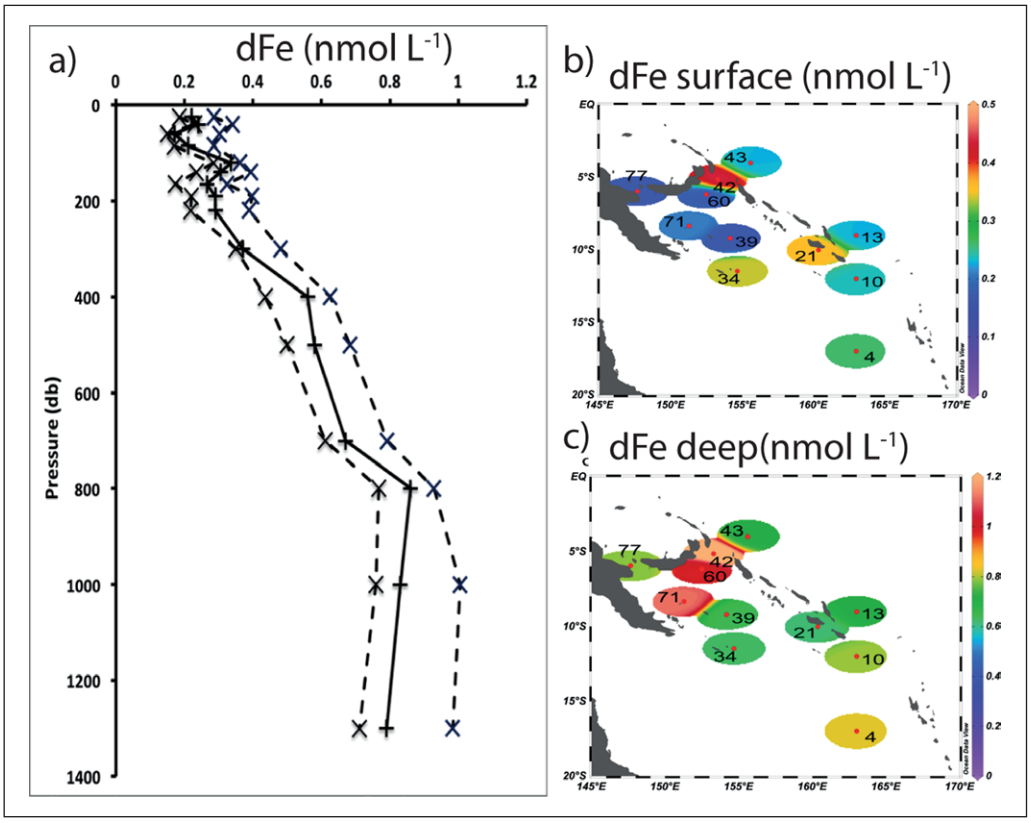

Figure 12: Dissolved iron concentrations during the Pandora cruise. (a) Vertical distribution showing the median dFe (solid line with crosses). The interquartile range, defined as the range around the median containing 50% of the data, is given between the two dotted lines. **(b)** Concentrations of dFe in surface waters measured during the Pandora cruise at 25 m for all the stations except station 34 (45 m) and 77 (80 m). **(c)** Same as (b), but at 1300 m. DOI: https://doi.org/10.1525/elementa.221.f12

isotopes (Lacan and Jeandel 2005; Grenier et al., 2013), currently underway The evolution of Al concentration along the NGCU pathways near the shallow shelf (<500 m) of the Rossel Island (station 34) suggests a noticeable source at about 400 m depth (**Figure 13**), at the core of the NGCU (Germineaud et al., 2016). There was a strong Mn gradient in the upper water column, also suggestive of sediment flux from the shelf (**Figure 13**). These stations also show evidence of enrichment at depth from deep sedimentary input.

The NGCU flows near the shallow sill along the Woodlark and Trobriand Islands (station 71) before it bifurcates into the NBCU. Here, there is an increase in aluminum and manganese at depth, as well as a peak in aluminum (but not manganese) around 500 m. This pattern could either be the signal from the Louisiades, or a lateral input from the nearby shallow sill. The absence of Mn enrichment at this depth suggests that the aluminum is from a more distant source like the Louisiades and that the Mn has been scavenged during transport. There is also deep water enrichment off of New Britain (station 60). In the Solomon Strait (station 42), the enrichment from the Louisiades is overwhelmed by the strong continental inputs through the strait.

Based on the Al profile, as the NBCU flows through the Solomon Strait it entrains both deep sedimentary inputs and lateral input from coastal margins. Continuing along the NGCU through the Vitiaz Strait (station 77), there are lateral inputs from the shelves, as well as enrichment at depth. Sites located adjacent to each other in the Solomon Strait (station 42) and northeast of Bougainville (station 43) are remarkably different. The Solomon Strait is enriched in aluminum and manganese relative to the Bougainville coast, suggesting that as water exits the Solomon Strait it flows more northwards than eastwards (**Figure 7**). This interpretation is consistent with ADCP findings, which show no flow between these neighboring sites. Rather, the Solomon Islands Coastal Undercurrent flows north, and there is some concurrence between this station and the south side of the Solomon Islands (station 13): they have similar Mn distributions, and similar Al distributions deep in the water column.

In the Coral Sea, upstream of the Solomon Sea, station 4 located within the North Caledonian Jet (NCJ) showed similar distributions of aluminum and manganese to those of station 82, further north. Lateral inputs from the shelf off New Caledonia enrich station 4 in both aluminum and manganese, relative to station 82. Based on these data, the predominant inputs of trace metals to the Solomon Sea are from coastal margin fluxes at depth, as well as lateral inputs in straits, where water is in contact with sediment at both the seafloor and along the coasts. There are high surface concentrations at many stations that reach thermocline depths (~300 m). In general, average

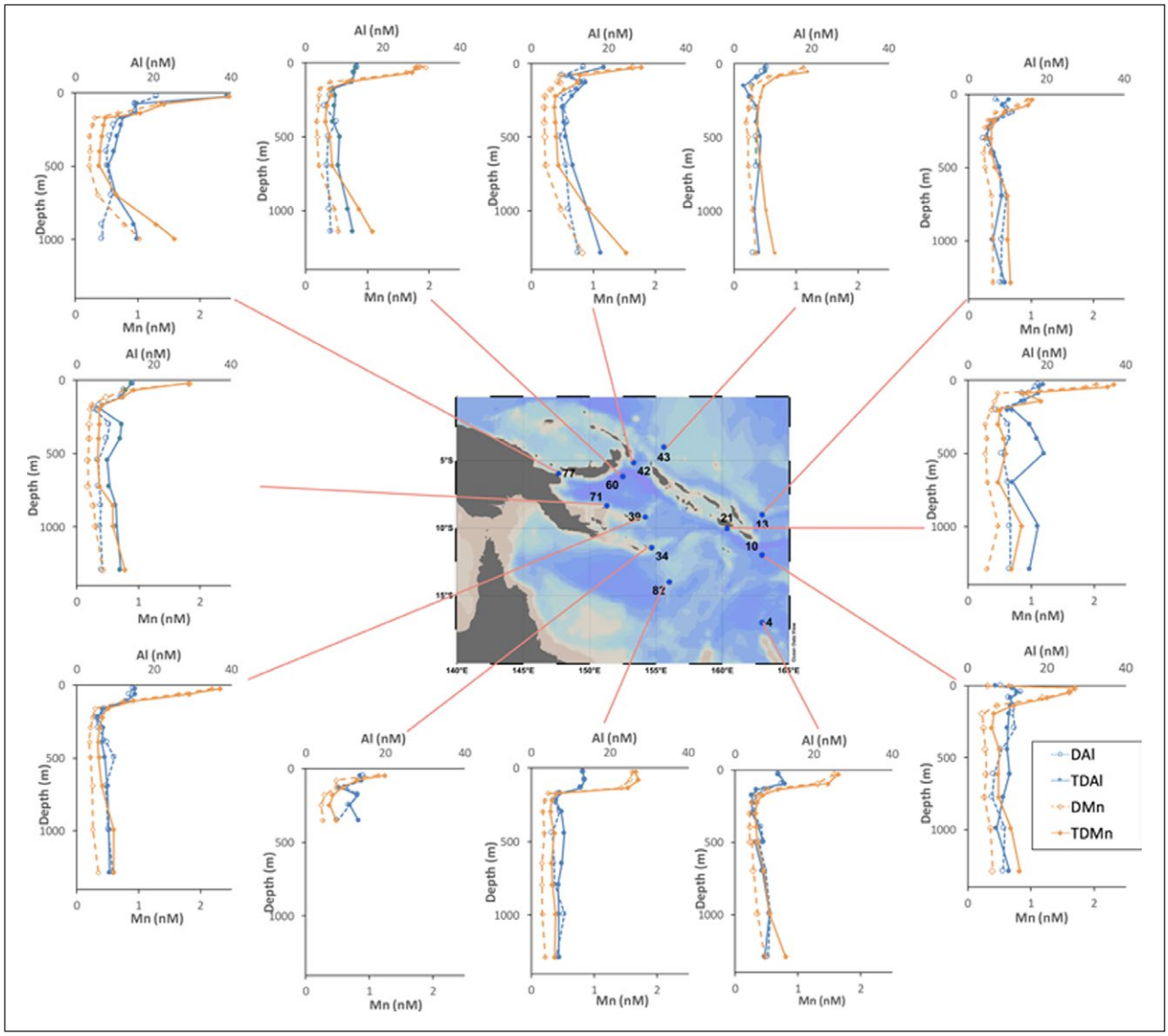

Figure 13: Aluminum and manganese distributions. dAl and dMn represent the dissolved fraction (< 0.2 μm), while tDAl and tDMn represent the unfiltered, whole water fraction. Both analysis were conducted after the acidification (pH 1.7–1.8). DOI: https://doi.org/10.1525/elementa.221.f13

aluminum and manganese concentrations (~12 nM and ~0.5 nM, respectively) are elevated relative to open ocean values. The most elevated concentrations in aluminum are found at station 77, along the outflow of the Vitiaz Strait, suggesting high terrestrial inputs in the surface waters.

The Solomon Sea is, in many locations, enriched in Al and Mn relative to open ocean values, suggesting that the interaction between strong currents and coastal boundaries is an important mechanism by which Al and Mn concentrations are enriched in this area. Such hypothesis will be confirmed, or not, when REE and Nd will be analyzed.

Mercury (Hg)

We present 9 vertical profiles (to 1300 m–depth) for tHg and MeHg that were sampled during the Pandora cruise. Total Hg concentrations varied only little, both vertically and horizontally (mean = 0.90 ± 0.18 pM, range = 0.55 – 1.69 pM, n = 87). The vertical tHg profiles showed neither a clear surface enrichment nor indications for sedimentary sources (**Figure 14**), and correspond to concentrations generally observed in the open ocean (Lamborg et al., 2014). The MeHg vertical distributions showed a similar pattern at all stations (mean = 0.17 ± 0.14 pM, range = 0.01 – 0.42 pM, n = 89).

MeHg concentrations were generally low (0.043 ± 0.021 pM, n = 39) at the surface (0–200 m), increase gradually from 200 to 400 m-depth (0.195 ± 0.103 pM, n = 21) to reach their maximum below 400 m-depth, (0.337 ± 0.034 pM, n = 29). The fact that MeHg and tHg distributions are relatively homogeneous in this dynamic zone and comparable to what has been observed eastward in the open Equatorial Pacific (Mason and Fitzgerald, 1990; Munson et al., 2015) suggests that MeHg is formed in situ in the oceanic water column and that boundary exchange has little or no influence. Concurrent near-margin Hg scavenging (Cossa et al., 2004) and Hg release

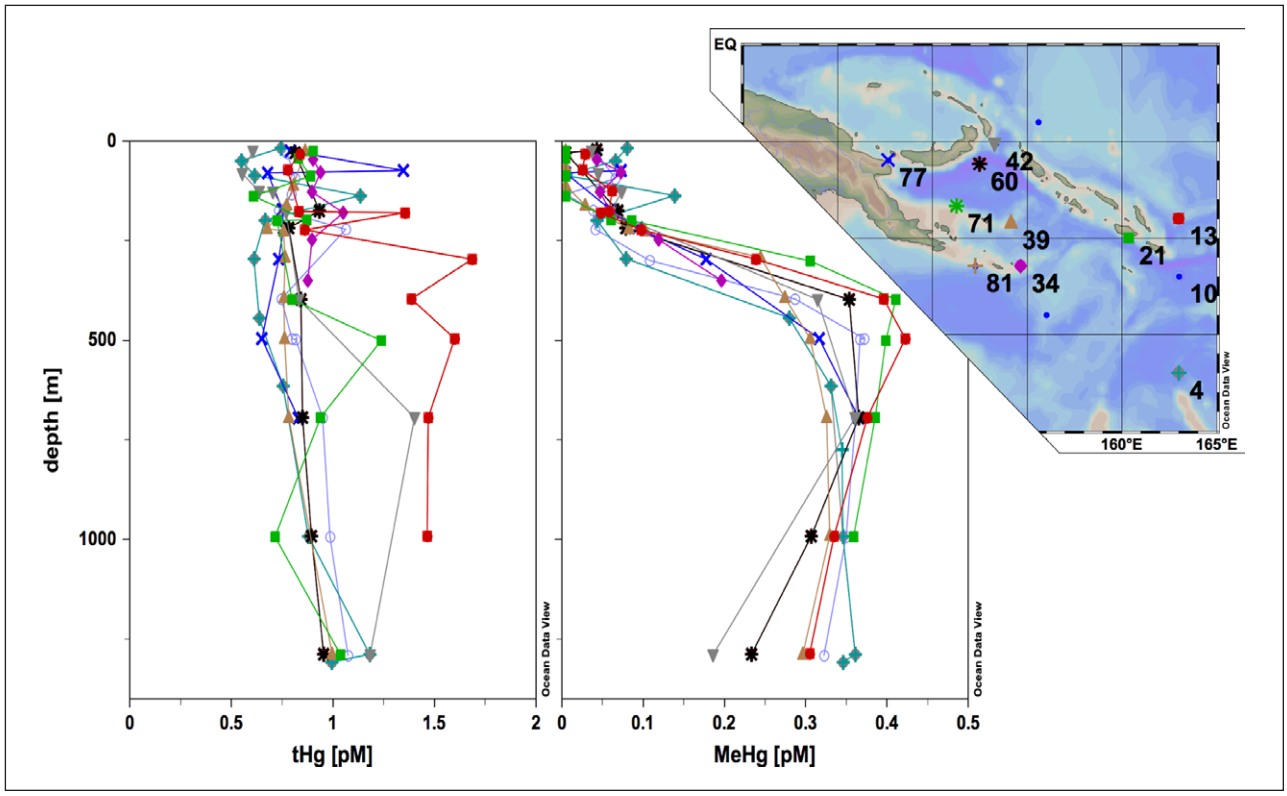

Figure 14: Mercury (Hg). Total Hg (tHg) and methylmercury (MeHg) distributions in picomoles per liter (pM) across the Solomon Sea. Color profiles correspond to color code stations on the map. DOI: https://doi.org/10.1525/elementa.221.f14

from margin sediments could indeed result in zero net effect on tHg concentrations. It is very unlikely, however, that those boundary exchange processes would not affect MeHg distributions.

Conclusions

The Pandora and MoorSPICE multidisciplinary cruises documented the Solomon Sea and part of the Coral and Bismarck Seas during two contrasted seasons, in austral winter (July–August 2012) and austral summer (March 2014). This paper presents the climatic context of the cruises, explains the scientific rationales behind all measurements made and describes the data acquisition. It presents an ensemble view of available observations and some initial results on physics, biogeochemistry and geochemistry so that those can be used as a reference for further, refined physical, geochemical and biogeochemical studies and stimulate multidisciplinary analyses.

Both cruises took place during neutral or weak ENSO conditions, and during weak active phases of MJO, precluding a strong influence of these phenomena on observed conditions. It is more likely that seasonal variability is the main driver of observed differences between the two cruises. Pandora took place during austral winter, and was associated with colder sea surface temperature, strong regional monsoonal wind forcing, and well-defined currents, whose transports were in the upper range of what had been previously estimated. In contrast, MoorSPICE took place in austral summer, and was associated with warm SSTs, much weaker winds, weaker currents and a greater activity of cyclonic eddies.

Measurements of temperature, salinity, oxygen, nutrients and currents allowed an unprecedented description of the fine-scale structure of water mass pathways, properties and mixing at different densities. Special attention was paid to the entrance and exits of the Solomon Sea, and these sections were sampled from top to bottom. Waters enter the Solomon Sea through the southern entrance in the narrow and deep NGCU confined to the western boundary, joining a weaker branch in mid-basin. This strong current further splits around islands and bifurcates on the New Britain coast, ultimately exiting the Solomon Sea through three narrow exits. The main branch exits northwestward through Vitiaz Strait, where the flow is found to extend to the bottom during both cruises. Other branches exit through St. Georges Channel and Solomon Strait. In the surface, waters also enter the Sea through Solomon Strait. Unexpected features include the deep extension of the currents, and strong contrasts between the interior of the Solomon Sea and conditions east of the Solomon Strait (Germineaud et al., 2016).

These energetic currents and the complex topography make this area potentially key for water mixing. Spatial patterns of mixing have been analyzed using CTD and LADCP profiles and reveal high seasonal dependence dissipation, which is much higher in the Solomon Sea than in other equatorial Pacific regions.

Biogeochemical measurements revealed new and important results. The Solomon Sea appears as a hot spot of N_2 fixation in the global ocean. *Trichodesmium* was quite abundant during both cruises and dominated the diazotroph community. N_2 fixation rates measured

were among the highest of the global ocean, especially in the narrow exits of the Solomon Sea where diazotrophs accumulated. The Pandora cruise carbon measurements also enabled the first evaluation of anthropogenic carbon and oceanic acidification in the Solomon Sea. Anthropogenic carbon signal penetrates deep in the water column, down to 1500 m, and acidification, large in the surface layer, was still found to be significant at 500 m depth.

Trace elements and isotopes were collected at selected locations along the water pathways; though many tracers are still currently being analyzed, the first results clearly reveal land to ocean inputs. A surface dissolved iron enrichment, probably due to river runoff or volcanic inputs, is confined close to the coasts (Labatut et al., 2014). Dissolved iron concentrations in deep waters suggest the existence of a deep sedimentary and/or hydrothermal source. Aluminum and manganese concentrations also suggest significant sediment flux from the shelf, in shallow and deep waters, and lateral inputs in the straits. Surprisingly, total mercury and methylmercury vertical distributions were similar to those in open ocean, and did not reveal any substantial surface enrichment, nor sedimentary sources. These results suggest that boundary exchange has little or no influence on MeHg formation. Further analyses of other tracers (more specifically REE concentrations and Nd isotopes) will help to constrain the nature and rate of the boundary exchanges at the land-ocean interface. The question of how these micronutrient elements will be transported downstream toward the equator remains open.

The data collected during these two cruises provide snapshots of the Solomon Sea conditions. They give unprecedented detailed information, but have inherent limitations, since a snapshot view of the currents can be strongly impacted by variability on many timescales, in particular by mesoscale eddies, intraseasonal or interannual variability. To complement these cruises, moorings have been deployed at the entrance and exits of the Solomon Sea (in Vitiaz Strait, St. Georges Channel and Solomon Strait) for a period of 18 months to 3 years. They sampled velocity, temperature and salinity at high frequency from top to bottom. Together with the repeated glider sections at the entrance of the Solomon Sea, with the PIES endpoint moorings, they will provide estimates of mass and heat transport variability from the tropics to the equator via the low-latitude western boundary current.

We hope to learn much from these observations about the scales of variability of this transport, which is a key element of the meridional subtropical cells supplying waters of mid to high latitude origin into the western equatorial Pacific. It is recognized that sustained boundary current observations are primary missing elements of the ocean observing system, and that their transport of mass, heat and freshwater should be monitored through dedicated observations (TPOS2020, report available online at http://tpos2020.org/first-report/). We also hope to learn from these measurements how to effectively built a sustained observing system for this region.

Appendix A: List of the trace elements and their isotopes for which samples were taken in the framework of PANDORA cruise

During Pandora (also GEOTRACES GP12), a comprehensive group of trace element samples were collected and are currently being measured. They are listed below, along with their scientific application:

1. Dissolved and particulate trace metal concentrations (Fe, Co, Mn, Cu, Zn, Pb, Cd) and some of their isotope distributions (Fe, Zn, Cu, Pb, Cd) will be used to assess the flux of trace elements provided to the water masses by their contact with the adjacent continent to the Solomon Sea. In addition, some of them as for example Fe, Co, Cu, or Zn are essential to the phytoplankton development and considered as micro-nutrients.
2. Concentrations and isotopic composition of these micronutrients help to constrain their origin, fate and cycling in seawater. For example, hydrothermal sources can provide iron that is isotopically light compared to the simple dissolution of erosion products, allowing the differentiation of the element sources (Radic et al., 2011; Conway and John, 2014; Labatut et al., 2014; Klar et al., 2017). Lead isotopes are good tracers of the lead sources in the different water masses.
3. Being conservative lithogenic tracers, particulate Al and ^{232}Th allow discrimination of the terrestrial from the biogenic fraction of the suspended material pool.
4. Radium and actinium isotopes (^{226}Ra, $T_{1/2}$ = 1602 years; ^{228}Ra, $T_{1/2}$ = 5.75 years; ^{224}Ra, $T_{1/2}$ = 3.66 day; ^{223}Ra, $T_{1/2}$ = 11.4 day) are all decay products of insoluble elements. Soluble, they often show high activity in shallow water overlying continental shelves via epibenthic outflux, and decrease in abundance by natural radioactive decay and mixing. Because of their chronometer properties, Ra isotopes provide information on water transit time and mixing processes (van Beek et al., 2008; Sanial et al., 2015).^{227}Ac (half-life of 21.8 years) is produced in the bottom sediments. ^{227}Ac will be analyzed on the same samples as for Ra and will help in constraining the vertical mixing on a longer time-scale (Geibert et al., 2002).
5. Rare Earth (REE) concentrations and Nd isotopes: The continental margins surrounding the world ocean display different isotopic signatures, reflecting their different geological origin. Old granitic sediments display low ^{143}Nd/^{144}Nd ratios while the volcanic sediment have high ^{143}Nd/^{144}Nd ratios. This property allows the quantification of the fraction of weathered material that dissolves at the continent/ocean interface (Arsouze et al., 2009; Jeandel and Oelkers, 2015). In addition, the distributions of Nd isotopic signatures and REE concentrations between the dissolved and particulate fractions of the collected samples are

complementary tracers that allow quantifying exchange processes between these two phases.

6. Thorium and protactinium isotopes: Thorium is insoluble in seawater. ^{228}Th and ^{230}Th are used as tracers of particle scavenging rates, settling rates and dissolved/particulate exchange (Henderson, 2003; Venchiarutti et al., 2008; Hayes et al., 2013; 2014). ^{231}Pa is also insoluble (but slightly more soluble than Th) and also produced in the water column by the decay of a soluble parent. Although more soluble than Th, ^{231}Pa is still particle reactive. Coupled with ^{230}Th isotope data, its distribution provides a powerful means to estimate dissolved/particle exchange rate, boundary scavenging and ventilation rates (Henderson, 2003; Venchiarutti et al., 2008; Hayes et al., 2013; 2014).
7. Stable Li and Pb isotopes: hydrothermal fluids have a characteristic stable Pb isotope signatures (as do Nd) that is altered near a vent. Li concentrations and Li isotopic signatures are also good specific tracers of hydrothermalism because seawater has an isotopic signature of about δ 7Li = +33‰ whereas hydrothermal fluids are close to δ 7 Li = +5−10‰.
8. Total Hg (tHg) and methylmercury (MeHg) are contaminants, the last one being accumulated and toxic for the trophic chain (Heimburger et al., 2015).

Data Accessibility Statement

1. Pandora data are freely available and can be accessed from SISMER and CYBER web server at http://www.obs-vlfr.fr/proof/php/pandora/pandora_overall.php.
2. MoorSPICE data are freely available and can be accessed from SISMER and CYBER web server at http://www.obs-vlfr.fr/proof/php/MoorSPICE/moorspice_overall.php.
3. R/V Mirai MR14–02 are freely available and can be accessed from the JAMSTEC data website http://www.godac.jamstec.go.jp/darwin/datatree/e.

Supplemental Files

The supplemental files for this article can be found as follows:

- **Figure S1.** Same as Figure 2 but for the Southwest Pacific. DOI: https://doi.org/10.1525/elementa.221.s1
- **Figures S2.** Same as Figure 4 but for the Southwest Pacific. DOI: https://doi.org/10.1525/elementa.221.s2
- **Figures S3.** Same as Figure 5 but for the Southwest Pacific. DOI: https://doi.org/10.1525/elementa.221.s3
- **Figures S4.** Same as Figure 7c, d but for the deep layers, from the shipboard ADCPs. DOI: https://doi.org/10.1525/elementa.221.s4
- **Figures S5.** (Upper) potential temperature and (lower) salinity section along 163E. White lines indicate isopycnals, dissolved oxygen and nitrate phosphate (no data available following a problem in the measurement system) and silicate. DOI: https://doi.org/10.1525/elementa.221.s5
- **Figures S6.** (Upper) potential temperature and (lower) salinity section east and inside Indispensable Strait, dissolved oxygen and nitrate, phosphate and silicate. DOI: https://doi.org/10.1525/elementa.221.s6
- **Figures S7.** (Upper) potential temperature and (lower) salinity section in the south entrance of the Solomon Sea dissolved oxygen and nitrate phosphate and silicate. DOI: https://doi.org/10.1525/elementa.221.s7
- **Figures S8.** (Upper) potential temperature and (lower) salinity section from Misima to Gizo islands dissolved oxygen and nitrate phosphate and silicate. DOI: https://doi.org/10.1525/elementa.221.s8
- **Figures S9.** (Upper) potential temperature and (lower) salinity section along the Solomon Strait and east Bougainville Island dissolved oxygen and nitrate phosphate and silicate. DOI: https://doi.org/10.1525/elementa.221.s9
- **Figures S10.** (Upper) potential temperature and (lower) salinity meridional section east of New Britain dissolved oxygen and nitrate phosphate and silicate. DOI: https://doi.org/10.1525/elementa.221.s10
- **Figures S11.** (Upper) potential temperature and (lower) salinity section along 152E dissolved oxygen and nitrate phosphate and silicate. DOI: https://doi.org/10.1525/elementa.221.s11
- **Figures S12.** (Upper) potential temperature and (lower) salinity section from Kiriwina to Madau Islands dissolved oxygen and nitrate phosphate and silicate. DOI: https://doi.org/10.1525/elementa.221.s12
- **Figures S13.** (Upper) potential temperature and (lower) salinity section along 150E dissolved oxygen and nitrate phosphate and silicate. DOI: https://doi.org/10.1525/elementa.221.s13
- **Figures S14.** (Upper) potential temperature and (lower) salinity section along Vitiaz Strait dissolved oxygen and nitrate phosphate and silicate. DOI: https://doi.org/10.1525/elementa.221.s14
- **Figures S15.** (Upper) potential temperature and (lower) salinity section in the south entrance of the Solomon Sea dissolved oxygen and nitrate phosphate and silicate. DOI: https://doi.org/10.1525/elementa.221.s15
- **Figures S16.** (Upper) potential temperature and (lower) salinity section along the Solomon Strait dissolved oxygen and nitrate phosphate and silicate. DOI: https://doi.org/10.1525/elementa.221.s16
- **Figures S17.** (Upper) potential temperature and (lower) salinity section along 152E dissolved oxygen and nitrate phosphate and silicate. DOI: https://doi.org/10.1525/elementa.221.s17
- **Figures S18.** (Upper) potential temperature and (lower) salinity section from Kiriwina to Madau Islands dissolved oxygen and nitrate phosphate and silicate. DOI: https://doi.org/10.1525/elementa.221.s18

- **Figures S19.** (Upper) potential temperature and (lower) salinity section along 150E dissolved oxygen and nitrate phosphate and silicate. DOI: https://doi.org/10.1525/elementa.221.s19
- **Figures S20.** (Upper) potential temperature and (lower) salinity section along Vitiaz Strait dissolved oxygen and nitrate phosphate and silicate. DOI: https://doi.org/10.1525/elementa.221.s20
- **Tables S1.** Summary of underway data acquisition. DOI: https://doi.org/10.1525/elementa.221.s21
- **Tables S2.** Summary of on-station data acquisition during Pandora. DOI: https://doi.org/10.1525/elementa.221.s22
- **Tables S3.** Summary of on-station data acquisition during MoorSPICE. DOI: https://doi.org/10.1525/elementa.221.s23

Acknowledgements

This work is a contribution to the CLIVAR/SPICE and GEOTRACES International programmes. We are grateful to the ship crews (RV *l'Atalante*, RV *Thompson* and RV *Mirai*) who made possible the various in situ measurements, thereby requiring skills and care. The collaboration with SOPAC/SPC, PI-GOOS, and University of Papua New Guinea was greatly appreciated. We thank the technical division of INSU (DT-INSU, O. Desprez de Gesincourt, L. Fichen, F. Perault, E. de Saint-Leger, C. Brachet and L. Souarnec); US-IMAGO (D. Lopez, L. Jamet), IRD Center Noumea (J. Carso, V. Perrin, C. Hartmann, J.-L. Fuda, D. Varillon), LEGOS support staff (B. Cournou, N. Lacroux, A. Baritaud, M. Mena) for their efforts to ensure a timely delivery of instruments/air tickets or participation at different stages of the cruise organization. We thank the Hydraulics Laboratory at SIO for their mooring expertise (P. Harvey, S. Kawamoto). We thank Patrick Raimbault (MIO) who did the mass spectrometric analyses related to biology. The Pandora data processing followed the US-IMAGO (IRD) information system (online at http://www.ird.fr/us191/spip.php?article66). Dissolved Fe analyses were funded by Labex Mer. Most geochemical graphics were made under ODV (Schlitzer, R., Ocean Data View, http://odv.awi.de, 2015). MoorSPICE data can be found through Cruise https://doi.org/10.7284/903044. Also thank C. Schmechtig who ensured the Pandora and MoorSPICE data delivery through the LEFE-CYBER Database (online at http://www.obs-vlfr.fr/proof/).

Funding information

The accomplishments were made possible through concurrent contributions of national funding agencies. The MoorSPICE and Pandora cruises have been co-funded by NSF grant OCE1029487, and by ANR project ANR-09-BLAN-0233-01 and INSU/LEFE project Solwara (IDAO and CYBER). Carbonate measurements were supported by European program FP7/CARBOCHANGE (grant 264879). NM thanks the Service National dAnalyses des Paramètres Océaniques du CO_2 (SNAPO-CO_2) supported by CNRS/INSU and UPMC (OSU ECCE-Terra). CG was supported by a PhD scholarship from the French Ministry of Research and Education. South Solomon Sea endpoint moorings (US NOAA funded CORC project grant NA10OAR432015) Mercury analyses were funded by ERC-2010-StG_20091028 grant from the European Research Council to JES.

Competing interests

The authors have no competing interests to declare.

Author Contributions

AG, SC, JS, CJ, and GE coordinated the projects, cruises and article writing. CG and MA contributed to the physical analysis and produced corresponding figures; MB, SB, HB, MR lead the biological analyses; JL the volcanic aspects. The geochemistry aspects were analyzed by NM (carbonates); L-EH (Hg); SM, JR (Al/Mn); FQ, GS, FL (Fe). Cruise data acquisition and treatment was ensured by JG and FB. TH lead the JAMSTEC cruise; WK, MK, EP, US, PV-B, MS and JES were involved at different stages of the results presented here.

References

Alberty, MS, Sprintall, J, MacKinnon, J, Ganachaud, A, Cravatte, S, et al. 2017 Spatial patterns of mixing in the Solomon Sea. *J Geophys Res, accepted.* DOI: https://doi.org/10.1002/2016JC012666

Allard, P, Aiuppa, A, Bani, P, Metrich, N, Bertagnini, A, et al. 2015 Prodigious emission rates and magma degassing budget of major, trace and radioactive volatile species from Ambrym basaltic volcano, Vanuatu island Arc. *Journal of Volcanology and Geothermal Research.* ISSN 03770273.

Alvarez, M, Lo Monaco, C, Tanhua, T, Yool, A, Oschlies, A, et al. 2009 Estimating the storage of anthropogenic carbon in the subtropical Indian Ocean: a comparison of five different approaches. *Biogeosciences* **6**(4): 681–703. ISSN 1726-4189.

Aminot, A and **Kerouel, R** 1995 Reference material for nutrients in seawater: stability of nitrate, nitrite, ammonia and phosphate in autoclaved samples. *Marine Chemistry* **49**(2–3): 221–232. ISSN 03044203.

Aminot, A and **Kerouel, R** 2007 *Dosage automatique des nutriments dans les eaux marines: méthodes en flux continu.* France: Ifremer. ISBN 9782759200238.

Arsouze, T, Dutay, JC, Lacan, F and **Jeandel, C** 2009 Reconstructing the Nd oceanic cycle using a coupled dynamical – biogeochemical model. *Biogeosciences Discussions* **6**(3): 5549–5588. ISSN 1810-6285.

Aufdenkampe, AK, McCarthy, JJ, Navarette, C, Rodier, M, Dunne, J, et al. 2002 Biogeochemical controls on new production in the tropical Pacific. *Deep Sea Research Part II: Topical Studies in Oceanography* **49**(13–14): 2619–2648. ISSN 09670645.

Bakker, DCE, Pfeil, B, Landa, CS, Metzl, N, O'Brien, KM, et al. 2016 A multi-decade record of high-quality fCO_2 data in version 3 of the Surface Ocean CO_2 Atlas (SOCAT). *Earth System Science Data* **8**(2): 383–413. ISSN 1866-3516.

Bani, P, Oppenheimer, C, Allard, P, Shinohara, H and **Tsanev, V,** et al 2012 First estimate of volcanic SO_2

budget for Vanuatu island arc. *Journal of Volcanology and Geothermal Research* **211**–**212**: 36–46. ISSN 03770273.

Benavides, M, Arístegui, J, Agawin, NS, Álvarez-Salgado, XA, Álvarez, M, et al. 2013 Low contribution of N_2 fixation to new production and excess nitrogen in the subtropical northeast Atlantic margin. *Deep Sea Research Part I: Oceanographic Research Papers* **81**: 36–48. ISSN 09670637.

Benavides, M and **Voss, M** 2015 Five decades of N_2 fixation research in the North Atlantic Ocean. *Frontiers in Marine Science* **2**. ISSN 2296-7745.

Berthelot, H, Benavides, M, Moisander, PH, Grososo, O and **Bonnet, S** 2017 Extremely high Nitrogen fixation rates in the particulate and dissolved pools in the Southwestern Pacific. *Geophys Res Lett* Submitted.

Bonnet, S, Berthelot, H, Turk-Kubo, K, Cornet-Barthaux, V, Fawcett, S, et al. 2016 Diazotroph derived nitrogen supports diatom growth in the South West Pacific: A quantitative study using nanoSIMS: Transfer of diazotrophic N into plankton. *Limnology and Oceanography* **61**(5): 1549–1562. ISSN 00243590.

Bonnet, S, Biegala, IC, Dutrieux, P, Slemons, LO and **Capone, DG** 2009 Nitrogen fixation in the western equatorial Pacific: Rates, diazotrophic cyanobacterial size class distribution, and biogeochemical significance. *Global Biogeochemical Cycles* **23**(3): n/a–n/a. ISSN 08866236.

Bonnet, S, Caffin, M, Berthelot, H and **Moutin, T** 2017 Hot spot of N_2 fixation in the western tropical South Pacific pleads for a spatial decoupling between N_2 fixation and denitrification. *Proceedings of the National Academy of Sciences* **114**(14): E2800–E2801. ISSN 0027-8424, 1091-6490. DOI: https://doi.org/10.1073/pnas.1619514114

Bonnet, S, Grosso, O and **Moutin, T** 2011 Planktonic dinitrogen fixation along a longitudinal gradient across the Mediterranean Sea during the stratified period (BOUM cruise). *Biogeosciences* **8**(8): 2257–2267. ISSN 1726-4189.

Bonnet, S, Guieu, C, Bruyant, F, Prasil, O, Van Wambeke, F, et al. 2008 Nutrient limitation of primary productivity in the Southeast Pacific (BIOSOPE cruise). *Biogeosciences* **5**(1): 215–225. ISSN 1726-4189.

Bonnet, S, Rodier, M, Turk-Kubo, KA, Germineaud, C, Menkes, C, et al. 2015 Contrasted geographical distribution of N_2 fixation rates and *nifH* phylotypes in the Coral and Solomon Seas (southwestern Pacific) during austral winter conditions. *Global Biogeochemical Cycles,* pp. n/a–n/a. ISSN 08866236.

Bostock, HC, Opdyke, BN and **Williams, MJ** 2010 Characterising the intermediate depth waters of the Pacific Ocean using ^{13}C and other geochemical tracers. *Deep Sea Research Part I: Oceanographic Research Papers* **57**(7): 847–859. ISSN 09670637.

Bourgeois, T, Orr, JC, Resplandy, L, Terhaar, J, Ethé, C, et al. 2016 Coastal-ocean uptake of anthropogenic carbon. *Biogeosciences* **13**(14): 4167–4185. ISSN 1726-4189.

Breitbarth, E, Oschlies, A and **LaRoche, J** 2007 Physiological constraints on the global distribution of Trichodesmium effect of temperature on diazotrophy. *Biogeosciences* **4**(1): 53–61. ISSN 1726-4189.

Church, M, Jenkins, B, Karl, D and **Zehr, J** 2005 Vertical distributions of nitrogen-fixing phylotypes at Stn Aloha in the oligotrophic North Pacific Ocean. *Aquatic Microbial Ecology* **38**: 3–14. ISSN 0948-3055, 1616-1564.

Conway, TM and **John, SG** 2014 Quantification of dissolved iron sources to the North Atlantic Ocean. *Nature* **511**(7508): 212–215. ISSN 0028-0836, 1476–4687.

Cossa, D, Cotte-Krief, MH, Mason, RP, Bretaudeau-Sanjuan, J 2004 Total mercury in the water column near the shelf edge of the European continental margin. *Marine Chemistry* **90**(1–4): 21–29. ISSN 03044203.

Cravatte, S, Ganachaud, A, Duong, QP, Kessler, WS, Eldin, G, et al. 2011 Observed circulation in the Solomon Sea from SADCP data. *Progress In Oceanography* **88**(1–4): 116–130. ISSN 00796611.

Daniel, A, Kérouel, R and **Aminot, A** 2012 Pasteurization: A reliable method for preservation of nutrient in seawater samples for inter-laboratory and field applications. *Marine Chemistry* **128**–**129**: 57–63. ISSN 03044203.

Davis, RE, Kessler, WS and **Sherman, JT** 2012 Gliders measure western boundary current transport from the South Pacific to the Equator. *Journal of Physical Oceanography* **42**(11): 2001–2013. ISSN 0022-3670, 1520-0485.

Delcroix, T, Radenac, MH, Cravatte, S, Alory, G, Gourdeau, L, et al. 2014 Sea surface temperature and salinity seasonal changes in the western Solomon and Bismarck Seas. *Journal of Geophysical Research: Oceans* **119**(4): 2642–2657. ISSN 21699275.

Dickson, A and **Millero, F** 1987 A comparison of the equilibrium constants for the dissociation of carbonic acid in seawater media. *Deep Sea Research Part A Oceanographic Research Papers* **34**(10): 1733–1743. ISSN 01980149.

Dickson, A and **Millero, F** 1989 Corrigenda. *Deep Sea Research Part A Oceanographic Research Papers* **36**(6): 983. DOI: https://doi.org/10.1016/0198-0149(89)90039-3

Djath, B, Melet, A, Verron, J, Molines, JM, Barnier, B, et al. 2014 A 1/36 model of the Solomon Sea embedded into a global ocean model: On the setting up of an interactive open boundary nested model system. *Journal of Operational Oceanography* **7**(1): 34–46. DOI: https://doi.org/10.1080/1755876X.2014.11020151

Djath, B, Verron, J, Melet, A, Gourdeau, L, Barnier, B, et al. 2014 Multiscale dynamical analysis of a high-resolution numerical model simulation of the

Solomon Sea circulation. *J Geophys Res Oceans.* ISSN 2169-9291.

Donguy, JR 1994 Surface and subsurface salinity in the tropical Pacific Ocean relations with climate. *Progress In Oceanography* **34**(1): 45–78. ISSN 0079-6611.

Donguy, JR and **Henin, C** 1977 Origin of the surface tropical water in the Coral and Tasman Seas. *Mar Freshwater Res* **28**(3): 321–332. DOI: https://doi.org/10.1071/MF9770321

Dore, JE, Brum, JR, Tupas, LM and **Karl, DM** 2002 Seasonal and interannual variability in sources of nitrogen supporting export in the oligotrophic subtropical North Pacific Ocean. *Limnology and Oceanography* **47**(6): 1595–1607. ISSN 00243590.

Fitzgerald, WF, Lamborg, CH and **Hammerschmidt, CR,** 2007 Marine Biogeochemical Cycling of Mercury. *Chemical Reviews* **107**(2): 641–662. ISSN 0009-2665, 1520-6890.

Ganachaud, A, Cravatte, S, Melet, A, Schiller, A, Holbrook, NJ, et al. 2014 The Southwest Pacific Ocean circulation and climate experiment (SPICE). *Journal of Geophysical Research: Oceans* **119**(11): 7660–7686. ISSN 21699275.

Gasparin, F, Ganachaud, A, Maes, C, Marin, F and **Eldin, G** 2012 Oceanic transports through the Solomon Sea: The bend of the New Guinea Coastal Undercurrent. *Geophysical Research Letters* **39**(15). ISSN 0094-8276.

Geibert, W, Rutgers van der Loeff, M, Hanfland, C, and **Dauelsberg, HJ** 2002 Actinium-227 as a deep-sea tracer: sources, distribution and applications. *Earth and Planetary Science Letters* **198**(1–2): 147–165. ISSN 0012821X.

Germineaud, C, Ganachaud, A, Sprintall, J, Cravatte, S, Eldin, G, et al. 2016 Pathways and water mass properties of the thermocline and intermediate waters in the Solomon Sea. *Journal of Physical Oceanography,* 1520–0485. ISSN 0022-3670.

Gourdeau, L, Verron, J, Melet, A, Kessler, W, Marin, F, et al. 2014 Exploring the mesoscale activity in the Solomon Sea: A complementary approach with a numerical model and altimetric data. *Journal of Geophysical Research: Oceans* **119**(4): 2290–2311. ISSN 21699275.

Grenier, M, Cravatte, S, Blanke, B, Menkes, C, Koch-Larrouy, A, et al. 2011 From the western boundary currents to the Pacific Equatorial Undercurrent: Modeled pathways and water mass evolutions. *Journal of Geophysical Research* **116**(C12): 044. DOI: https://doi.org/10.1029/2011JC007477

Grenier, M, Jeandel, C and **Cravatte, S** 2014 From the subtropicss to the equator in the Southwest Pacific: Continental material fluxes quantified using neodymium data along modeled thermocline water pathways. *Journal of Geophysical Research: Oceans* **119**(6): 3948–3966. ISSN 21699275.

Grenier, M, Jeandel, C, Lacan, F, Vance, D, Venchiarutti, C, et al. 2013 From the subtropics to the central equatorial Pacific Ocean: Neodymium isotopic composition and rare earth element concentration variations. *Journal of Geophysical Research.* ISSN 0148-0227.

Gruber, N 2004 The Dynamics of the Marine Nitrogen Cycle and its Influence on Atmospheric CO_2 Variations, In: Follows M, Oguz T, (eds.), *The Ocean Carbon Cycle and Climate.* Dordrecht: Springer Netherlands: pp. 97–148. ISBN 978-1-4020-2086-5, 978-1-4020-2087-2. DOI: https://doi.org/10.1007/978-1-4020-2087-2_4

Halm, H, Lam, P, Ferdelman, TG, Lavik, G, Dittmar, T, et al. 2012 Heterotrophic organisms dominate nitrogen fixation in the South Pacific Gyre. *The ISME Journal* **6**(6): 1238–1249. ISSN 1751-7362, 1751-7370.

Hayes, CT, Anderson, RF, Fleisher, MQ, Serno, S, Winckler, G, et al. 2014 Biogeography in $^{231}Pa/^{230}Th$ ratios and a balanced ^{231}Pa budget for the Pacific Ocean. *Earth and Planetary Science Letters* **391**: 307–318. ISSN 0012821X.

Hayes, CT, Anderson, RF, Jaccard, SL, François, R, Fleisher, MQ, et al. 2013 A new perspective on boundary scavenging in the North Pacific Ocean. *Earth and Planetary Science Letters* **369–370**: 86–97. ISSN 0012821X.

Heimburger, LE, Sonke, JE, Cossa, D, Point, D, Lagane, C, et al. 2015 Shallow methylmercury production in the marginal sea ice zone of the central Arctic Ocean. *Scientific Reports* **5**: 10318. ISSN 2045-2322.

Henderson, GM 2003 The U-series Toolbox for Paleoceanography. *Reviews in Mineralogy and Geochemistry* **52**(1): 493–531. ISSN 1529-6466.

Holbrook, NJ and **Maharaj, AM** 2008 Southwest Pacific subtropical mode water: A climatology. *Progress in Oceanography* **77**(4): 298–315. ISSN 00796611.

Hristova, HG and **Kessler, WS** 2012 Surface circulation in the Solomon Sea derived from Lagrangian drifter observations. *Journal of Physical Oceanography* **42**(3): 448–458. ISSN 0022-3670, 1520-0485.

Hristova, HG, Kessler, WS, McWilliams, JC and **Molemaker, MJ** 2014 Mesoscale variability and its seasonality in the Solomon and Coral Seas. *Journal of Geophysical Research: Oceans.* ISSN 21699275.

Hydes, DJ, Aoyama, M, Aminot, A, Bakker, K, Becker, S, et al. 2010 Recommendations for the determination of nutrients in seawater to high kevels of precision and inter-comparability using continuous flow analysers. version 1: GO-SHIP.ORG.

Jeandel, C and **Oelkers, EH** 2015 The influence of terrigenous particulate material dissolution on ocean chemistry and global element cycles. *Chemical Geology* **395**: 50–66. ISSN 00092541.

Karl, D, Letelier, R, Tupas, L, Dore, J, Christian, J, et al. 1997 The role of nitrogen fixation in biogeochemical cycling in the subtropical North Pacific Ocean. *Nature* **388**(6642): 533–538. ISSN 0028-0836.

Karl, D, Michaels, A, Bergman, B, Capone, D, Carpenter, E, et al. 2002 Dinitrogen fixation in the

world's oceans. *Biogeochemistry* **57**–**58**(1): 47–98. ISSN 0168-2563.

Kawabe, M and **Fujio, S** 2010 Pacific ocean circulation based on observation. *Journal of Oceanography* **66**(3): 389–403. ISSN 0916-8370, 1573-868X.

Kessler, WS and **Cravatte, S** 2013 Mean circulation of the Coral Sea. *Journal of Geophysical Research: Oceans* **118**(12): 6385–6410. ISSN 21699275.

Klar, JK, James, RH, Gibbs, D, Lough, A, Parkinson, I, et al. 2017 Isotopic signature of dissolved iron delivered to the Southern Ocean from hydrothermal vents in the East Scotia Sea. *Geology* **45**(4): 351–354. DOI: https://doi.org/10.1130/G38432.1

Labatut, M, Lacan, F, Pradoux, C, Chmeleff, J, Radic, A, et al. 2014 Iron sources and dissolved-particulate interactions in the seawater of the Western Equatorial Pacific, iron isotope perspectives. *Global Biogeochemical Cycles* **28**(10): 1044–1065. ISSN 08866236.

Lacan, F and **Jeandel, C** 2005 Neodymium isotopes as a new tool for quantifying exchange fluxes at the continent–ocean interface. *Earth and Planetary Science Letters* **232**(3–4): 245–257. ISSN 0012821X.

Lamborg, CH, Hammerschmidt, CR, Bowman, KL, Swarr, GJ, Munson, KM, et al. 2014 A global ocean inventory of anthropogenic mercury based on water column measurements. *Nature* **512**(7512): 65–68. ISSN 0028-0836, 1476-4687.

Langdon, C. 2010 Determination of dissolved oxygen in Seawater by Winkler Titration using the Amperometric Technique. version 1: GO-SHIP.ORG.

Lauvset, SK, Key, RM, Olsen, A, van Heuven, S, Velo, A, et al. 2016 A new global interior ocean mapped climatology: the 1° × 1° GLODAP version 2. *Earth System Science Data Discussions*. pp. 1–30. ISSN 1866-3591.

Le Bouteiller, A 2003 Primary production, new production, and growth rate in the equatorial Pacific: Changes from mesotrophic to oligotrophic regime. *Journal of Geophysical Research* **108**(C12). ISSN 0148-0227.

Lee, HT 2014 Climate Algorithm Theoretical Basis Document (C-ATBD): Outgoing Longwave Radiation (OLR) – Daily. NOAA's Climate Data Record (CDR) program. Technical Report CDRP-ATBD-0526, 46 p.

Lefevre, J, Menkes, C, Bani, P, Marchesiello, P, Curci, G, et al. 2015 Distribution of sulfur aerosol precursors in the SPCZ released by continuous volcanic degassing at Ambrym, Vanuatu. *Journal of Volcanology and Geothermal Research* ISSN 03770273.

Lenton, A, Tilbrook, B, Matear, RJ, Sasse, TP and **Nojiri, Y** 2016 Historical reconstruction of ocean acidification in the Australian region. *Biogeosciences* **13**(6): 1753–1765. ISSN 1726-4189.

Le Quéré, C, Moriarty, R, Andrew, RM, Canadell, JG, Sitch, S, et al. 2015 Global Carbon Budget 2015. *Earth System Science Data* **7**(2): 349–396. ISSN 1866-3516.

Lindstrom, E, Lukas, R, Fine, RA, Godfrey, JS, Meyers, G, et al. 1987 The western equatorial Pacific Ocean circulation study. *Nature* **330**: 533–537. DOI: https://doi.org/10.1038/330533a0

Luo, YW, Doney, SC, Anderson, LA, Benavides, M, Berman-Frank, I, et al. 2012 Database of diazotrophs in global ocean: abundance, biomass and nitrogen fixation rates. *Earth System Science Data* **4**(1): 47–73. ISSN 1866-3516.

Madden, RA and **Julian, PR** 1972 Description of global-scale circulation cells in the tropics with a 40–50 day period. *J Atmos Sci* **29**(6): 1109–1123. ISSN 0022-4928.

Mari, X, Lefèvre, J, Torréton, JP, Bettarel, Y, Pringault, O, et al. 2014 Effects of soot deposition on particle dynamics and microbial processes in marine surface waters. *Global Biogeochemical Cycles* **28**(7): 662–678. ISSN 08866236.

Mason, RP, Choi, AL, Fitzgerald, WF, Hammerschmidt, CR, Lamborg, CH, et al. 2012 Mercury biogeochemical cycling in the ocean and policy implications. *Environmental Research* **119**: 101–117. ISSN 00139351.

Mason, RP and **Fitzgerald, WF** 1990 Alkylmercury species in the equatorial Pacific. *Nature* **347**(6292): 457–459. ISSN 0028-0836.

McCartney, M 1977 Subantarctic Mode Water. *Deep Sea Research, supplement* **24**: 103–119.

McCormick, BT, Edmonds, M, Mather, TA and **Carn, SA** 2012 First synoptic analysis of volcanic degassing in Papua New Guinea: VOLCANIC DEGASSING IN PAPUA NEW GUINEA. *Geochemistry, Geophysics, Geosystems* **13**(3): n/a–n/a. ISSN 15252027.

McPhaden, MJ, Timmermann, A, Widlansky, MJ, Balmaseda, MA and **Stockdale, TN** 2015 The curious case of the El Nino that never happened: A perspective from 40 years of progress in climate research and forcasting. *Bulletin of the American Meteorological Society* **96**(10): 1647–1665. ISSN 0003-0007, 1520-0477.

Mehrbach, C, Culberson, CH, Hawley, JE and **Pytkowicx, RM** 1973 Measurement of the apparent dissociation constants of carbonic acid in seawater at atmospheric pressure. *Limnology and Oceanography* **18**(6): 897–907. ISSN 00243590.

Melet, A, Gourdeau, L, Kessler, WS, Verron, J and **Molines, JM** 2010 Thermocline circulation in the Solomon Sea: A modeling study. *J Phys Oceanogr* **40**(6): 1302–1319. ISSN 0022-3670.

Melet, A, Gourdeau, L, Verron, J and **Djath, B** 2013 Solomon Sea circulation and water mass modifications: response at ENSO timescales. *Ocean Dynamics* **63**(1): 1–19. ISSN 1616-7341, 1616-7228.

Melet, A, Verron, J, Gourdeau, L and **Koch-Larrouy, A** 2011 Equatorward pathways of Solomon Sea water masses and their modifications. *Journal of Physical Oceanography* **41**: 810–826. DOI: https://doi.org/10.1175/2010JPO4559.1

Menkes, CE, Lengaigne, M, Vialard, J, Puy, M, Marchesiello, P, et al. 2014 About the role of Westerly Wind Events in the possible development of an El Nino in 2014. *Geophysical Research Letters* **41**(18): 6476–6483. ISSN 00948276.

Metzl, N, Corbiere, A, Reverdin, G, Lenton, A, Takahashi, T, et al. 2010 Recent acceleration of the sea surface CO_2 growth rate in the North Atlantic subpolar gyre (1993–2008) revealed by winter observations. *Global Biogeochemical Cycles* **24**(4): n/a–n/a. ISSN 08866236.

Moisander, PH, Beinart, RA, Hewson, I, White, AE, Johnson, KS, et al. 2010. Unicellular cyanobacterial distributions broaden the oceanic N_2 fixation domain. *Science* **327**(5972): 1512–1514. ISSN 0036-8075, 1095-9203.

Moisander, PH, Beinart, RA, Voss, M and **Zehr, JP** 2008 Diversity and abundance of diazotrophic microorganisms in the South China Sea during intermonsoon. *The ISME Journal* **2**(9): 954–967. ISSN 1751-7362, 1751-7370.

Moutin, T, Van Den, BB, Beker, B, Dupouy, C, Rimmelin, P, et al. 2005 Phosphate availability controls *Trichodesmium* spp. biomass in the SW Pacific Ocean. *Marine Ecology Progress Series* **297**: 15–21. ISSN 0171-8630, 1616-1599.

Munson, KM, Lamborg, CH, Swarr, GJ and **Saito, MA** 2015 Mercury species concentrations and fluxes in the Central Tropical Pacific Ocean. *Global Biogeochemical Cycles* **29**(5): 656–676. ISSN 08866236.

Nagamoto, C, Parungo, F, Kopcewicz, B and **Zhou, MY** 1990 Chemical analysis of rain samples collected over the Pacific Ocean. *Journal of Geophysical Research* **95**(D13): 22343. ISSN 0148-0227.

Nelson, DM, Tréguer, P, Brzezinski, MA, Leynaert, A and **Quéguiner, B** 1995 Production and dissolution of biogenic silica in the ocean: Revised global estimates, comparison with regional data and relationship to biogenic sedimentation. *Global Biogeochemical Cycles* **9**(3): 359–372. ISSN 1944-9224.

Olsen, A, Key, RM, van Heuven, S, Lauvset, SK, Velo, A, et al. 2016 The Global Ocean Data Analysis Project version 2 (GLODAPv2) – an internally consistent data product for the world ocean. *Earth System Science Data* **8**(2): 297–323. ISSN 1866-3516.

Orsi, AH, Johnson, GC and **Bullister, JL** 1999 Circulation, mixing and production of Antarctic Bottom Water. *Prog Oceanogr* **43**(1): 55–109. DOI: https://doi.org/10.1016/S0079-6611(99)00004-X

Pena, MA, Lewis, MR and **Cullen, JJ** 1994 New production in the warm waters of the tropical Pacific Ocean. *Journal of Geophysical Research* **99**(C7): 14255. ISSN 0148-0227.

Pierrot, DE, Lewis, A and **Wallace, D** 2011 MS Excel Program Developed for CO_2 system calculations. ORNL/CDIAC-105a. Oak Ridge, Tennessee: Oak Ridge National Laboratory, U.S. Department of Energy.

Qu, T and **Lindstrom, EJ** 2002 A Climatological Interpretation of the Circulation in the Western South Pacific. *J Phys Oceanogr* **32**(9): 2492–2508. ISSN 0022-3670.

Qu, T and **Lindstrom, EJ** 2004 Northward Intrusion of Antarctic Intermediate Water in the Western Pacific. *J Phys Oceanogr* **34**(9): 2104–2118. ISSN 0022-3670.

Radic, A, Lacan, F and **Murray, JW** 2011 Iron isotopes in the seawater of the equatorial Pacific Ocean: New constraints for the oceanic iron cycle. *Earth and Planetary Science Letters* **306**(1–2): 1–10. ISSN 0012-821X.

Raimbault, P and **Garcia, N** 2008 Evidence for efficient regenerated production and dinitrogen fixation in nitrogen-deficient waters of the South Pacific Ocean: impact on new and export production estimates. *Biogeosciences* **5**(2): 323–338. ISSN 1726-4189.

Raven, JA 1988 The iron and molybdenum use efficiencies of plant growth with different energy, carbon and nitrogen sources. *New Phytologist* **109**(3): 279–287. ISSN 0028-646X, 1469-8137.

Resing, JA and **Measures, CI** 1994 Fluorometric Determination of Al in Seawater by Flow Injection Analysis with In-Line Preconcentration. *Anal Chem* **66**(22): 4105–4111. ISSN 0003-2700.

Resing, JA and **Mottl, MJ** 1992 Determination of manganese in seawater using flow injection analysis with on-line preconcentration and spectrophotometric detection. *Anal Chem* **64**(22): 2682–2687. ISSN 0003-2700.

Ridame, C, Dekaezemacker, J, Guieu, C, Bonnet, S, L'Helguen, S, et al. 2014 Contrasted Saharan dust events in LNLC environments: impact on nutrient dynamics and primary production. *Biogeosciences* **11**(17): 4783–4800. ISSN 1726-4189.

Sanial, V, van Beek, P, Lansard, B, Souhaut, M, Kestenare, E, et al. 2015 Use of Ra isotopes to deduce rapid transfer of sediment-derived inputs off Kerguelen. *Biogeosciences* **12**(5): 1415–1430. ISSN 1726-4189.

Saout-Grit, C, Ganachaud, A, Maes, C, Finot, L, Jamet, L, et al. 2015 Calibration of CTD oxygen data collected in the Coral Sea during the 2012 bifurcation cruise. *Mercator Ocean-Coriolis Quarterly Newsletter Special Issue* **52**(3): 27–33.

Sarthou, G, Baker, AR, Kramer, J, Laan, P, Las, A, et al. 2007 Influence of atmospheric inputs on the iron distribution in the subtropical northeast Atlantic Ocean. *Marine Chemistry* **104**(3–4): 186–202. ISSN 03044203. DOI: https://doi.org/10.1016/j.marchem.2006.11.004

Shiozaki, T, Kodama, T, Kitajima, S, Sato, M and **Furuya, K** 2013 Advective transport of diazotrophs and importance of their nitrogen fixation on new and primary production in the western Pacific warm pool. *Limnology and Oceanography* **58**(1): 49–60. ISSN 00243590.

Slemons, LO, Murray, JW, Resing, J, Paul, B and **Dutrieux, P** 2010 Western Pacific coastal sources of iron, manganese, and aluminum to the Equatorial Undercurrent: Western Pacific metal sources to the EUC. *Global Biogeochemical Cycles* **24**(3): n/a–n/a. ISSN 08866236.

Sokolov, S and **Rintoul, S** 2000 Circulation and water masses of the southwest Pacific: WOCE section P11, Papua New Guinea to Tasmania. *Journal of marine research* **58**(2): 223–268. DOI: https://doi.org/10.1357/002224000321511151

Suzuki, T, Ishii, M and **Christian, J** 2013 PACIFICA Data Synthesis Project. ORNL/CDIAC-159, NDP-092. Environmental Sciences Division, Oak Ridge National Laboratory,Tennessee: Carbon Dioxide Information Analysis Center (CDIAC).

Takahashi, T, Sutherland, S, Chipman, D, Goddard, J, Ho, C, et al. 2014 Climatological distributions of pH, pCO_2, total CO_2, alkalinity, and $CaCO_3$ saturation in the global surface ocean, and temporal changes at selected locations. *Marine Chemistry* **164**: 95–125. ISSN 03044203.

Touratier, F, Azouzi, L and **Goyet, C** 2007 CFC-11, ^{14}C and ^{3}H tracers as a means to assess anthropogenic CO_2 concentrations in the ocean. *Tellus B* **59**(2): 318–325. ISSN 0280-6509, 1600-0889.

Tsimplis, MN, Bacon, S and **Bryden, HL** 1998 The circulation of the sub-Tropical South Pacific derived from hydrographic data. *J Geophys Res* **103**(C10): 21,443–21,468. DOI: https://doi.org/10.1029/98JC01881

Tsuchiya, M, Lukas, R, Fine, RA, Firing, E and **Lindstrom, E** 1989 Source waters of the Pacific Equatorial Undercurrent. *Progress In Oceanography* **23**(2): 101–147. ISSN 0079-6611.

Uchida, H, Johnson, CG and **McTaggart, KE** 2010 CTD oxygen sensor calibration procedures. version 1: GO-SHIP.ORG.

van Beek, P, Bourquin, M, Reyss, JL, Souhaut, M, Charette, M, et al. 2008 Radium isotopes to investigate the water mass pathways on the Kerguelen Plateau (Southern Ocean). *Deep Sea Research Part II: Topical Studies in Oceanography* **55**(5–7): 622–637. ISSN 09670645.

Venchiarutti, C, Jeandel, C and **Roy-Barman, M** 2008 Particle dynamics study in the wake of Kerguelen Island using thorium isotopes. *Deep Sea Research Part I: Oceanographic Research Papers* **55**(10): 1343–1363. ISSN 09670637.

Vetch, P and **Haefeli, S** 1997 August visit reveals lava fountains, Strombolian explosions, Ambrym. *Bull Global Volc Network* **22**: 11.

Visbeck, M 2002 Deep velocity profiling using Acoustic Doppler Current Profilers: Bottom tracks and inverse solutions. *J Atm Oc Tech* **19**: 794–807. DOI: https://doi.org/10.1175/1520-0426(2002)019<0794:DVPULA>2.0.CO;2

Wheeler, MC and **Hendon, HH** 2004 An All-Season Real-Time Multivariate MJO Index: Development of an Index for Monitoring and Prediction. *Mon Wea Rev* **132**(8): 1917–1932. ISSN 0027-0644.

Wyrtki, K 1962 The subsurface water masses in the western South Pacific Ocean. *Marine and Freshwater Research* **13**(1): 18–47. DOI: https://doi.org/10.1071/MF9620018

Yoshikawa, C, Nakatsuka, T and **Kawahata, H** 2005 Transition of low-salinity water in the Western Pacific Warm Pool recorded in the nitrogen isotopic ratios of settling particles. *Geophysical Research Letters* **32**(14): n/a–n/a. ISSN 00948276.

How to cite this article: Ganachaud, A, Cravatte, S, Sprintall, J, Germineaud, C, Alberty, M, Jeandel, C, Eldin, G, Metzl, N, Bonnet, S, Benavides, M, Heimburger, L-E, Lefèvre, J, Michael, S, Resing, J, Quéroué, F, Sarthou, G, Rodier, M, Berthelot, H, Baurand, F, Grelet, J, Hasegawa, T, Kessler, W, Kilepak, M, Lacan, F, Privat, E, Send, U, Van Beek, P, Souhaut, M and Sonke, JE 2017 The Solomon Sea: its circulation, chemistry, geochemistry and biology explored during two oceanographic cruises. *Elem Sci Anth,* 5: 33, DOI: https://doi.org/10.1525/elementa.221

Domain Editor-in-Chief: Jody W. Deming, University of Washington, US

Associate Editor: Eddy C. Carmack, Fisheries and Oceans Canada, CA

Knowledge Domain: Ocean Science

Submitted: 26 August 2016 **Accepted:** 19 April 2017 **Published:** 30 June 2017

ELEMENTA Science of the Anthropocene

Elem Sci Anth is a peer-reviewed open access journal published by University of California Press.

OPEN ACCESS